THESIS

DESIGN, MODELING, AND OPTIMIZATION OF 3D PRINTED COMPLIANT MECHANISMS WITH APPLICATIONS TO MINIATURE WALKING ROBOTS

Submitted by

Anthony R. DeMario

Department of Mechanical Engineering

In partial fulfillment of the requirements

For the Degree of Master of Science

Colorado State University

Fort Collins, Colorado

Summer 2018

Master's Committee

Advisor: Jianguo Zhao

Mitchell Stansloski
Anthony Maciejewski

ABSTRACT

DESIGN, MODELING, AND OPTIMIZATION OF 3D PRINTED COMPLIANT MECHANISMS WITH APPLICATIONS TO MINIATURE WALKING ROBOTS

Miniature robots have many applications ranging from military surveillance to search and rescue assistance in disaster areas. Traditionally, fabrication of these robots has been labor-intensive, time-consuming, and expensive. This thesis proposes to leverage recent advances in 3D printing technology to fabricate centimeter-scale walking robots utilizing compliant elements printed directly into the walking mechanisms in replacement of traditional revolute joints or rigid links. The ability to design around the capabilities of 3D printers and novel material choices gives miniature robots the ability to have multiple functions in the same mechanism, reduces the overall number of parts that must be assembled to make a functional robot, and decrease the time and cost of prototyping.

This thesis details three areas of study for compliant mechanisms with applications to walking robots. First, we utilize multi-material 3D printing to fabricate a miniature walking robot ($49 \times 38 \times 25mm$) that directly replaces the traditional revolute joints in the designed walking mechanism with a custom, soft joint. Some links are also printed with soft materials to enhance the robustness and durability of the robot. Along with design and testing of the robot, we develop two numerical models to simulate the effects of the soft elements on the mechanism trajectory. Second, we leverage the numerical models to optimize the design of the walking mechanism to produce a trajectory similar to that of the same mechanism using all revolute joints. Third, we redesign the original robot to utilize a conductive polylactic acid (PLA) material to 3D print linkages that allow for changing joints locations by softening the desired part through applied electricity. This variable joint mechanism can create multiple trajectories without changing the mechanical structure, therefore creating a multi-functional compliant mech-

anism. Such capabilities are demonstrated through walking on the ground and grasping objects using the same leg mechanism.

ACKNOWLEDGEMENTS

I would like to thank my advisor, Dr. Zhao, for being patient and working hard with me to achieve this milestone accomplishment. I would like to thank my committee members Mitchell Stansloski and Prof. Anthony Maciejewki for helping to review and edit this thesis paper. I would like to thank Fathom and the I2P lab for providing all the 3D printed parts for this project. I would like to thank the CSU Department of Mechanical Engineering for providing funding for my graduate studies and the resources to achieve the successful completion of this research. Finally, I would like to thank my friends and family for giving me support throughout this entire process. I am truly blessed.

TABLE OF CONTENTS

LIST OF TABLES

LIST OF FIGURES

Chapter 1

Introduction

Miniature robots with a size of a few centimeters have a wide variety of applications. Equipped with appropriate sensors (e.g., cameras), they can be deployed in disaster areas to search for survivors. With their small sizes providing good camouflage, they are ideal platforms for military surveillance. Since they can be built with relatively low costs, many of them can also be deployed to form mobile sensor networks for dynamic environmental monitoring.

Due to their advantages, many small robots that can walk, crawl, and fly have been built in recent years. Since this thesis is focused on small walking robots, only existing miniature robots with walking capabilities will be reviewed. The RoACH robot, actuated with shape memory alloy coils and with a size of 3cm and a mass of 2.4g, can walk with hexapedal legs at a speed of 3 cm/s [4]. Later, the same group improved their design to be able to overcome obstacles [5]. They have also designed a DC motor actuated version called DASH [6] which can run at a speed up to 1.5 m/s. The HAMR robot is driven by piezoelectric actuators and has a mass of 1.7 g and a body length of 4.7 cm. With six legs made of flexure-based spherical five-bar mechanisms, it can locomote at a speed of 0.44 m/s [7]. A 1.6 g, 2 cm quadrupedal robot with external magnetic actuations was developed to explore various gaits for insect-size miniature robots [8].

To build these small robots, new fabrication methods have been proposed to create mechanisms with rigid links and soft joints. Smart composite microstructures (SCM) process [9] was developed to fabricate the RoACH, DASH, and the HAMR (see Fig. 1.2). This process sandwiches sheets of flexible material between sheets of rigid materials, for which the flexible material becomes rotational joints, while rigid materials form the links. Shape Deposition Manufacturing (SDM) can be employed to fabricate parts with multiple materials by first depositing and then removing appropriate materials in sequence [10]. This method has been used to fabricate robotic hands [11] and running robots [12]. Multi-Material Molding (MMM) is developed with multiple steps of molding to combine soft materials with rigid materials [13], which has been

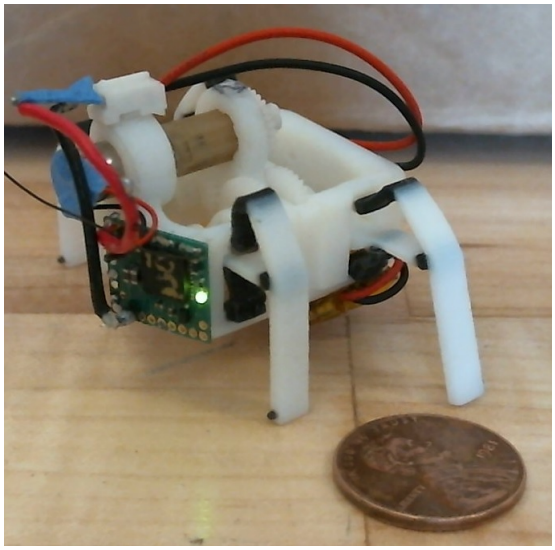

Figure 1.1: Miniature walking robot fully assembled next to a U.S. penny

used for flapping-wing robots [14]. Recently, the laser cut elastomer refill (LaCER) method was proposed to fabricate miniature compliant mechanisms by first using lasers to cut rigid materials and then filling selectively removed sections with elastomer materials [15]. This method has been employed to fabricate miniature walking robots [16].

This thesis presents a design for a new miniature walking robot (a prototype is shown in Fig. 1.1) that can be directly printed using existing 3D printing technology (PolyJet, Stratasys, Ltd and Proto-Pasta). The robot is enabled by four identical linkages as four legs. Each linkage employs soft materials in place of both traditional joints and rigid links. Compared to existing fabrication methods, directly using 3D printings has two advantages. First, the fabrication process is without human intervention, and thus easier and faster. In fact, with appropriate designs, 3D printers can directly print both soft and rigid materials in a single part. Second, a variety of materials can be chosen for different performance requirements. As a result, the soft components can have different characteristics depending on design requirements.

This thesis focuses on two specific types and materials of 3D printing. First is multi-material 3D printing (MM3P) which gives the ability to print complex parts with varying materials to reduce the overall number of parts required for a mechanism. There current are seven different

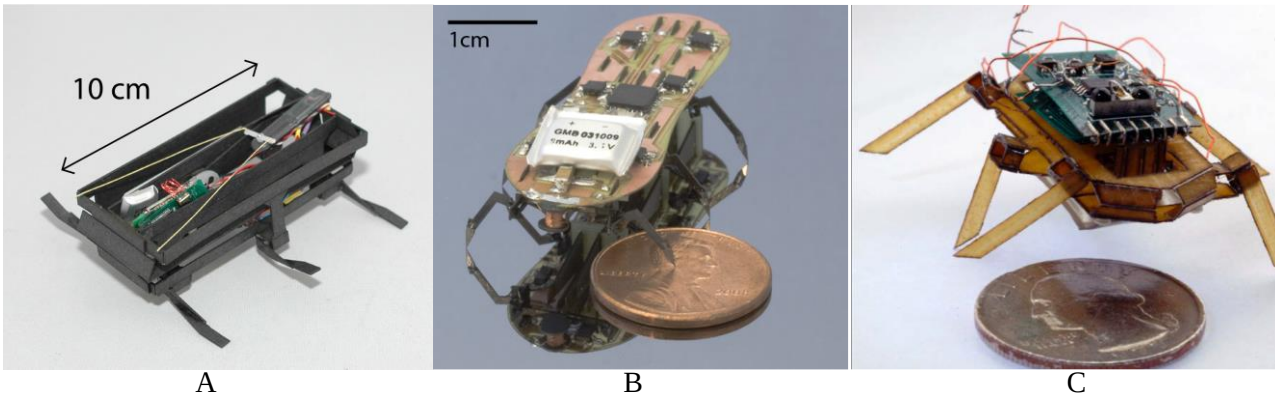

Figure 1.2: Existing miniature walking robots based on non-traditional manufacturing and assembly methods: A) DASH B) HAMR C) RoACH

durometers of soft materials available on the printer used in the following research. Due to the advantage of MM3P, it has recently been utilized in building novel devices and robots. Gaynor *et al.* have investigated the compliant mechanisms enabled by MM3P and the associated optimization problems [17]. Bruyas *et al.* have designed a soft revolute joint with a large amplitude using MM3P [18] and built an interventional device using several such joints [19]. Using MM3P, Bartlett *et al.* have developed a jumping robot that has a soft exterior but a rigid core [20]. Second is traditional spool feed desktop 3D printers. While this technology has been around for a number of years and is reaching maturity, innovations in printer material has allowed for further development of the manufacturing method. Conductive materials open up the possibility of achieving a variable purpose mechanism that can be produced in an inexpensive and timely fashion.

There are two major contributions for this thesis. First, it investigates the concept of both soft joints and links for compliant mechanisms and demonstrate the concept with a functional walking robot prototype fabricated using both MM3P and traditional methods. Although mechanisms with soft components have been investigated in the field of compliant mechanisms [16, 21] and used in various miniature robots (e.g, flying [14, 22], walking [4–6], etc.), to the best of our knowledge, mechanisms with both soft joints and links have never been investigated before, which will potentially inspire the design and realization of novel miniature mechanisms

for a wide range of applications including robotics, deployable structures, or mechanical metamaterials. Second, it details the development several numerical methods to predict the motion of mechanisms with many soft components, which has been not investigated before as most of existing studies only investigated a single soft component [21, 23]. Such a numerical method can serve as a basis for more general and in-depth theoretical investigations (e.g., dynamics) for mechanisms with soft components.

This thesis is broken into three sections. Chapter 2 presents a miniature walking robot utilizing MM3D. The chapter details the design of the custom walking mechanism and four legged robot utilizing the mechanism, the fabrication process for the robot, the numerical modeling techniques used to simulate soft component deformation, and the results of the prototype testing and model validation. Chapter 3 details the optimization process used to further enhance the design of the walking mechanism through numerical simulation. The optimized mechanism is able to closely simulate the path of a revolute joint mechanism trajectory, giving insight into the use of soft joints to replace revolute joints in existing mechanisms. Chapter 4 presents a miniature robot that utilizes a new material to create a compliant mechanism with multiple functions. The chapter details the preliminary study of the use of conductive PLA, softened by applying voltage, to create a single mechanism that can change its trajectory between a walking motion and gripping motion without altering the mechanism in any way. This is achieved by selecting various sections of the rigid linkages to be either compliant or rigid depending on the applications. Results show concept feasibility and two practical applications using the mechanism designed in the previous chapters and discussion of future research applications.

Chapter 2

A Multi-Material 3D Printable Miniature Walking Robot

The development of MM3P has opened the door to designed many features into miniature robots that are either impossible or too expensive using previous manufacturing methods. This chapter details the design, fabrication and numerical modeling of a 3D printed miniature walking robot utilizing both soft joint and soft links.

The first aspect of this project is the design of the miniature walking robot that could take advantage of MM3P to incorporate compliant features into the walking mechanism. The design objective of this miniature walking robot contains two main aspects. First, achieve biomimetic walking motion with a single actuator driving four legs. For this objective, we employ a series of linkages to accomplish the desired trajectory of each leg as linkages can produce complicated and precise motion if properly designed. In this case, seven joints and six links are required for each leg to achieve the walking motion. To use a single actuator, an appropriate gear train has to be designed to coordinate each legs' motion. Second, as a miniature robotic platform, the overall size of robot should be in centimeter scale. The limitations of MM3P will not allow effective components with dimensions less than a millimeter and therefore limit how small the robot can be. Keeping within the centimeter scale also allows this robot to be compared against existing walking robots.

The second aspect is the fabrication of the robot. This takes advantage of a 3D printer by Stratasys to take the design and print the desired robot. Special care was taken to ensure that all aspects of the robot would allow the parts to print to the specs required. Materials were chosen to allow for the greatest range of motion of each soft component, dimensions confirmed to be within spec of the machine and tolerances for other assembled components were checked in test prints.

The third aspect is the numerical modeling of the soft components in the robot and specifically the walking mechanism. Since the design is based around replacing all traditional revolute joints in the walking mechanism with a non-linear, compliant joint, and some of the rigid links with compliant links, the resulting trajectory of the mechanism will differ from the originally designed linkage. Understanding how these soft components bend and stretch to accomplish the desired motion allows for further study into the use of such materials in compliant mechanisms. To accomplish this, a study of the implementation of two different modeling approaches to approximating the deformation is presented. The first model used is the Psuedorigid-body 1R (PRB 1R) model. This model is more basic, modeling the soft components as two rigid links and a revolute joint located some distance along the soft component. The second model studied is the Three Spring Rotational-Prismatic-Rotational (RPR) model. This model replicates the components as a series of three links connected by springs to approximate forces and deformation.

The fourth aspect is validating the numerical models and the functional capabilities of the robot. A series of experiments using a variety of test parameters and setups show the accuracy of the models for multiple configurations of the robot and walking test prove the basic capabilities of the robot to locomote under its own weight and in a fully wireless fashion.

2.1 Design

The overall design of the robot illustrated in Fig. 2.1 has a crab-like stance with four legs that are a derivative of the Klann mechanism [24], a drive train with six gears, four drive links coupling the legs to the drive train, and a single planetary geared micro DC motor. Although the ultimate goal for the project is to directly print out all the components of the robot as a single part including the drive train, in this first step of the research only the four legs and the robot body are printed together, after which the drive train is manually assembled. As 3D printing technology advances, it will be more feasible to print the gears, drive links, and axles, requiring only the motor to be installed for the robot to be functional. The overall dimensions of the robot

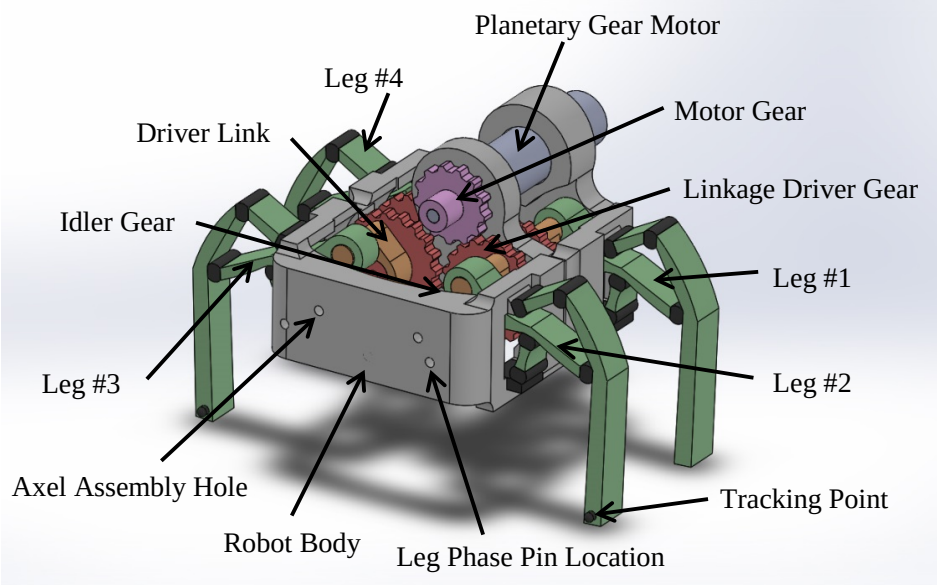

Figure 2.1: 3D model of miniature walking robot

are $49mm \times 33mm \times 25mm$ and weights just $14g$ with the motor, battery and wireless controller, making it comparable in size and weight to other robots in the miniature scale discussed in the Introduction.

2.1.1 Leg Mechanism

To achieve the biomimetic walking motion required for stable robot locomotion, the basis for the leg mechanism for this robot is the Klann mechanism, which can simulate the gait of legged animals and insects while being relatively simple and easy to alter [24]. A configuration of the mechanism that produced a long, flat section of the trajectory where the foot was in contact with the ground was chosen as it allowed a simple reconfiguration of the ground joints to allow the mechanism to be printed with the base while not being highly dependent on the link lengths to still produce the desired trajectory. As shown in Fig. 2.2, the mechanism schematic shows six rigid links and seven revolute joints. Joint 1 is driven by the output from the drive train, while Joint 2 is realized by a pin-hole structure using the driver link shown in Fig. 2.3. Except these two joints, all the other five joints are realized as identical soft joints.

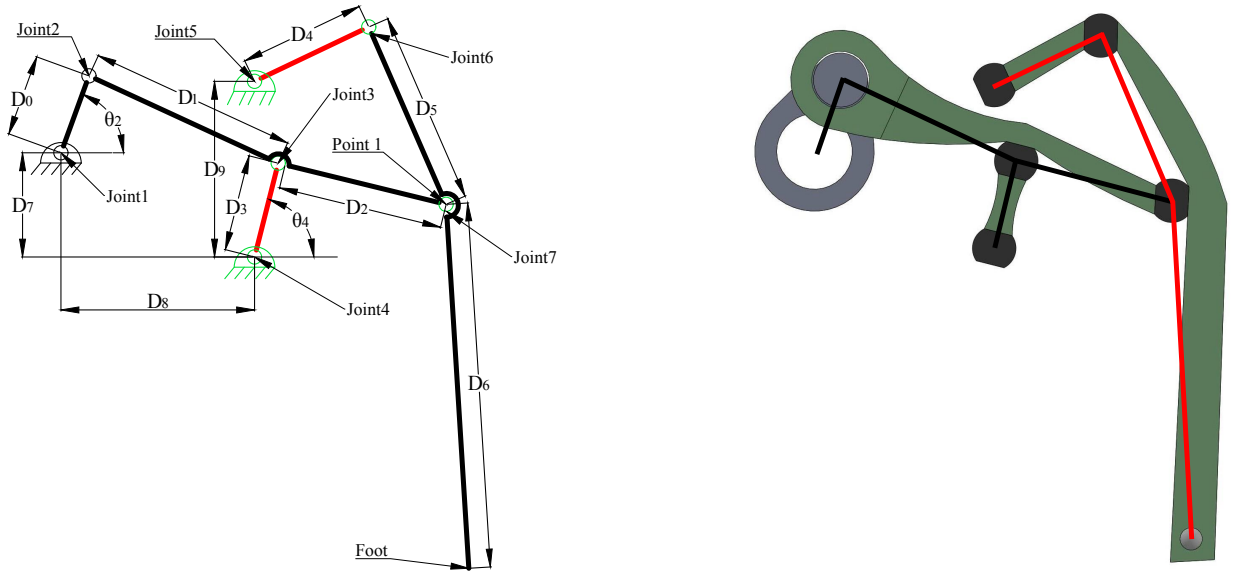

Figure 2.2: Leg mechanism schematic (a) and 3D print model (b) shown with generic dimension locations. Links D_3 and D_4 are the soft links in the second configuration of the mechanism.

The schematic in Fig. 2.2 shows all the dimensions locations as well as joint numbers and specific points (Point 1 and Foot) in the mechanism, whose trajectories will be analyzed in the modeling section and tracked during experiments as well as a side by side comparison of the 3D model vs the traditional linkage schematic. The black links indicate the initial four-bar mechanism that is used to solve for the trajectory of Point 1 and the red links show the remainder of the leg mechanism used to solve for the foot path. To minimize the overall size of the mechanism, reduce the maximum deflection angle of the soft joints, and maintain a satisfactory foot path, the dimensions shown in Fig. 2.2 were chosen as follows: D_0 = 3.4375mm, D_1 = 8.75mm, D_2 = 7.26mm, D_3 = 4.06mm, D_4 = 5.31mm, D_5 = 8.13mm, D_6 = 15.31mm, D_7 = 4.38mm, and D_8 = 8.13mm.

Two configurations of the mechanism are designed. The first is a soft joint only configuration. This replaces joints 3-7 with soft joints and all links remain rigid. This configuration tries to best replicate the original mechanism by only replacing the revolute joints with soft joints. All the soft joints in the mechanism are identical and designed with a flat section on each side to match up with any of the links. The design allows for symmetric motion as the joint is deformed

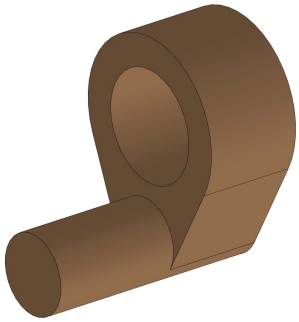

Figure 2.3: 3D model of Drive Link

in both clockwise and counterclockwise directions during one cycle of the drive link. Each soft joint in the mechanism is printed with the same material and geometry to allow for simpler mathematical modeling. Future adjustments to our joint models could include investigating the effects of different materials being used at different joint locations. With the accuracy and tolerance restrictions put on the design by the 3D printer used, the size of the soft joint is not arbitrarily small and it was chosen as: $1.5mm$ at the widest by $1.0mm$ between flat sections by $4mm$ deep.

The second configuration of the mechanism keep the same joints soft and replaces links D_3 and D_4 with a soft link. This configuration allows for a continuation of the study into longer, soft links and how they impact the functionality of the mechanism. Both links retain the same geometry as the first configuration but are printed using a slightly harder soft material than the joint. This ensures that the link is able to retain shape and transmit forces during locomotion while still remaining soft.

2.1.2 Leg Motion and Gait Pattern

The mechanism design in Sec. 2.1.1 generates a foot path similar to that of long-legged animals and insects. Fig. 2.4 shows three foot trajectories: (a) is the designed mechanism trajectory, (b) is the foot path for both a front and hind leg of a spider [1], and (c) shows the foot path of a horse [2]. This comparison shows that this foot path is suited for locomotion of a platform that

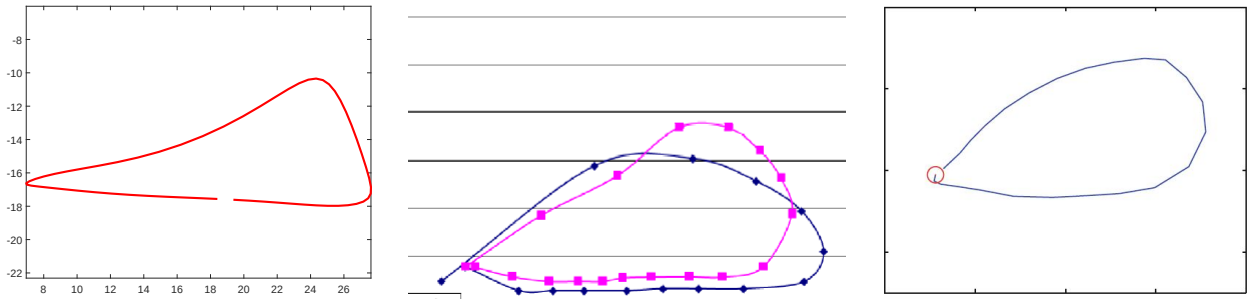

(a) **(b)** **(c)**

Figure 2.4: Designed leg trajectory (a), spider leg trajectory [1] (b), horse leg trajectory [2] (c)

contains at least four legs in a variety of configurations and can function with a variety of gait patterns found in nature.

To walk efficiently over ground, the motion of the four legs needs to be coordinated. A leg phase offset based on four-legged locomotion presented by Morita [25] is used to best replicate the gait patterns found in nature for slow, stable locomotion. Each drive link is offset by 90 degrees from the other legs, shown visually in Fig. 2.5. Starting with the leg directly driven by the motor (leg 2) whose drive link is at -90 degrees from horizontal, the adjoining leg (leg 1) is offset 180 degrees from leg 2 with an angle of $+90$ degrees from the horizontal. Leg 3, which is on the same side of the robot as leg 2, is at 0 degrees from horizontal and its adjoining leg (leg 4) is at $+180$ degrees. Such an angle offset is chosen to match the “amble" gait of a legged animal or insect as it keeps two feet on the ground at all times while one is lifting off the ground and the fourth is returning to the ground [25]. This also allows for a wide range of speeds from the motor to drive the legs and still have stable locomotion with minimal rocking. To guarantee the desired phase angle, four assembly holes are designed into the robot body so that small pins (leg phase pin in Fig. 2.1) can be used to assemble the drive link with each leg. With such a design, only one gait pattern can be set on a single robot using the assembly holes designed into the robot body, but by adjusting the location of the holes or adding additional holes, other gait patterns could be investigated.

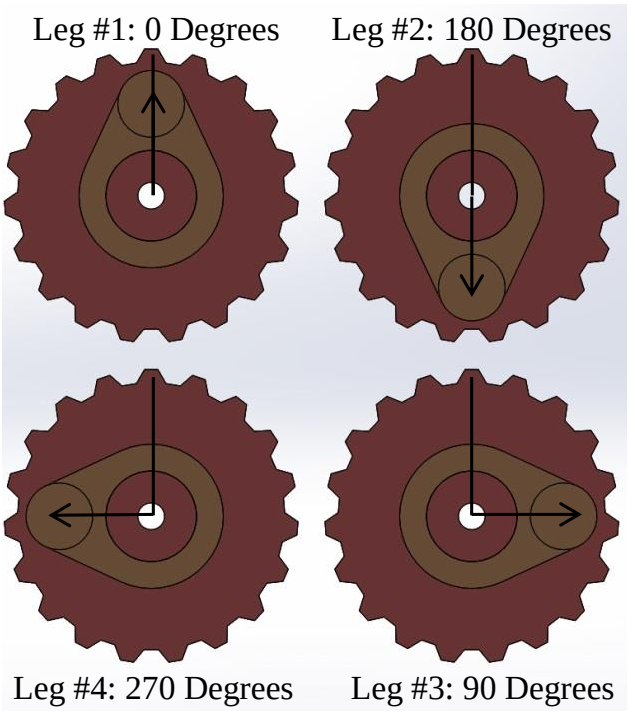

Figure 2.5: Visual representation of the individual leg offset need to achieve the desired walking gait pattern

2.2 Fabrication

The printing of the robot components was performed by Fathom (studiofathom.com). The legs and body of the robot are printed using a Objet 500 Connex 3 [1] multi-material 3D printer using PolyJet Flex 27A material for the soft joints, PolyJet Flex 50A for the soft links, and VeroWhitePlus for rigid links and robot body [2]. The Objet 500 has a stated resolution of 600 dpi in both X and Y and 1600 dpi in Z (0.042 mm and 0.016 mm respectfully) and an accuracy of 0.2 mm. 27A was chosen as the material for the soft joints because it is the most ductile material offered in the 3D printer used. The material has similar elastic properties to hydrated human skin with an elastic modulus of approximately $1.3e5$ Pa [26], which is the only material property that is significant in both modeling processes. 50A was used for the soft links as it has an approx elastic modu-

[1] http://www.stratasys.com/3d-printers/objet-350-500-connex3

[2] www.stratasysdirect.com/materials/polyjet

lus twice that of 27A, offering the mechanism more stability than the 27A while still deforming under the forces provided by the motor. Table 2.1 has a breakdown of the material properties provided by the manufacturer that were used to chose mechanism materials.

Table 2.1: Table of PolyJet material specifications from manufacturer

Mechanical Property	27A	40A	50A	60A
Tensile Strength	$0.8-1.5MPa$	$0.5-1.5MPa$	$0.5-1.5MPa$	$2.0-4.0MPa$
Elongation at Break	170-220%	150-170%	130-150%	80-100%
Shore Hardness	22-32	35-45	45-55	55-65
Simulated Product	Skin	Latex Gloves	Door Seal	Pencil Eraser

The drive train shown in Fig. 2.6 has six plastic gears which transfer power from the DC motor (Part #:GH612s from Gizmozone) to all four legs. At the end of the drive train, each leg is driven by a drive gear (Part #:GS0.3-36 from Gizmoszone) with a drive link (Fig. 2.1). The beginning of the gear train is the motor gear (Part #:GS0.3-28 from Gizmoszone) which is press-fitted onto the motor shaft. This drives the drive gear for Leg 2 which is meshed with the idler gear (Part #:GS0.3-10 from Gizmoszone) located at the bottom of the robot. $1mm$ stainless steel rodes from McMaster Carr are used as the axles for the drive gears and idler gear. This idler gear, which spans both sides of the gear train, transfers power not only to Leg 3 but also to the other set of legs (Legs 1 and 4) and is required because for forward walking motion, all drive links must be driven in the same direction.

2.3 Modeling

The soft materials being used in the custom leg mechanisms have not previously been studied in a dynamic environment like the constant and repetitive bending and stretching occurring during the motion of a walking mechanism. For this reason, it is necessary that the deformation properties of the materials be studied and modeled to predict the motion of a dynamic sys-

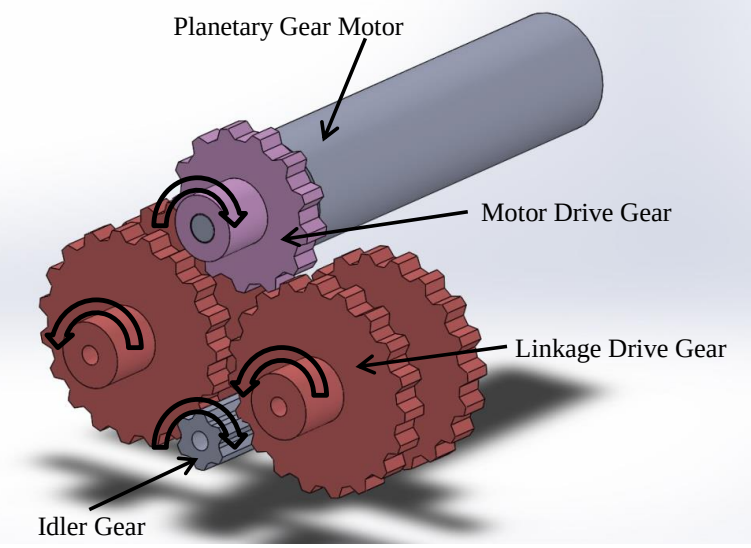

Figure 2.6: MM3P robot gear train

tem that utilized these materials. The most readily studied compliant mechanism is the long, slender elastic beam. To fall under this realm of modeling, the length of the beam must be at least four times longer than its height [21]. If this is the case, the deformation of the beam is considered linear and therefore does not requires numerical approximation. However, the soft components designed for this project have a length to width ratio of less than one and the soft links have a ratio of approximately 2. This causes both the joints and links to deform in a non-linear fashion. For this reason a numerical model needs to be developed to study and predict the behavior of the soft components of a mechanism.

There are two different modeling approaches used to study the soft components of the mechanism. First is a modified Psuedorigid-body 1R model (PRB 1R). This model approximates a soft component by replacing the continuous member with two rigid links and an ideal revolute joint. The traditional 1R model assumes that the location of the revolute joint along the length of the soft component is fixed for a given geometry and material . However, the design of the soft components falls just out of the bound this model is traditionally applied to and therefore it was hypothesized and is confirmed through experimental results that the location of this rotational center varies during deformation. The modified PRB 1R model calculates the trajec-

tory of the soft components with this variable instantaneous center of rotation. The gain of this model is that it is simple to introduce into the model and requires very little time to calculate. However, it is not able to capture extension or compression or an inflection point in the curve of a soft component. The second modeling approach studied is the Three Spring Rotational-Prismatic-Rotational (RPR) model. This model approximates a soft component with two rigid links connected in the middle by a prismatic joint and two revolute joints. This model adds the ability to account for significant elongation effects and a single inflection point within the deflection curve. The drawback to this model is that with the additional effects to account for, the calculation time is significantly increased over the 1R model.

The following assumptions are made for all modeling studied in this paper:

- All designed dimensions are used as exact dimensions because the printed dimensions of any mechanism or part have smaller errors from designed dimensions than the error introduced in the experimental data collection process.
- All motion occurs in the plane of the mechanism, all forces act in the plane of the mechanism, and all moments act perpendicular to the plane of the mechanism.
- All rigid materials used are infinitely stiff.
- The elastic moduli of the soft materials used are the same for each joint and each link, respectfully.
- The elastic moduli of the soft materials used are homogeneous and isotropic within each soft joint and soft link.

Regardless of the modeling approach used, the general process for the numerical simulation of the motion of the compliant mechanism goes as follows. First, the mechanism is assumed to have all ideal, revolute joints and a vector loop analysis is performed to calculate the angles each joint will deform as well as the angle of the forces acting at each joint through one revolution of the drive link. Second, large beam deflection equations (Sec. 2.3.1) are used in an iterative

loop to determine the forces and moments applied to each soft component in the mechanism to achieve the joint angles calculated from the ideal model. Third, the forces and moments are used in the PRB 1R model (Sec. 2.3.2) and the RPR model (Sec. 2.3.3) to determine the trajectory of each soft component according to its location and orientation within the mechanism. The trajectories of all the components of the mechanism are combined together to solve for the trajectory of the end of the mechanism. The numerical modeling trajectory vs experimental trajectory vs ideal model trajectory with the associated error bounds and observations for a mechanism containing soft joints and rigid links is presented in Sec. 2.4.1 and for a mechanism containing both soft joint and soft links is presented in Sec. 2.4.2.

2.3.1 Solving Force and Moment for Each Soft Element using Large Deflection Beam Equations

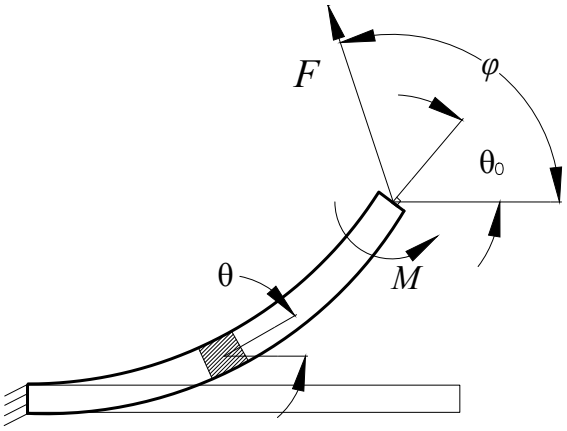

Figure 2.7: Large Deflection Beam model showing variable setup

For any soft component in the mechanism, as the drive link rotates, the tip of any soft element in the leg mechanism will be subject to a force F and moment M, which will determine the element's deformation. The goal in this subsection is to solve F and M to be used as input to the RPR or PRB 1R model.

Suppose F is applied at an angle of ϕ, and the soft element deflects at an angle of θ_0, then we can model the deformation using the equations for a large deflection beam [27]:

$$\sqrt{a} = \frac{1}{2}\int_0^{\theta_0} \frac{d\theta}{\sqrt{\cos(\theta_0 - \phi) - \cos(\theta - \phi) + \kappa}} \tag{2.1}$$

$$\kappa = \frac{b^2}{4a} \quad \text{with} \quad a = \frac{Fl^2}{2EI}, \quad b = \frac{Ml}{EI} \tag{2.2}$$

where θ_0 is the deflection angle for the beam, ϕ is the angle for force F, κ is the load ratio as defined in [27], E is the Elastic Modulus of the material, I is area moment of inertia, and l is the length of the beam. In general, it is impossible to solve F and M because there are more unknowns (ϕ, θ_0, F, and M) than equations (only one). To simplify the problem, we consider an ideal mechanism when all the joints are ideal revolute ones and all links are rigid ones. In this case, given a drive link angle, we can use traditional vector loop equations for planar mechanisms [28] to solve the force angle ϕ and the deflection angle θ_0 for each joint/link. At the same drive link angle, if the drive joint torque is given, we can also solve F and M applied at each joint/link using the static analysis for planar mechanisms [28]. Our numerical procedure to find F and M for each soft element is based on such observations. Given a drive link angle, we will iteratively find the drive torque to first solve ϕ and θ_0, F, and M, and then plug them into the large deflection beam equation to ensure the equation will hold. Then the resulting F and M will be considered as the solution. Note that the assumption for using the ideal mechanism to solve for F and M is reasonable since the mechanism with soft elements should resemble a trajectory similar to the ideal mechanism, although some errors might exist.

All the soft joints in the leg mechanism are geometrically identical. Two of them (Joint 4 and 5 in Fig. 2.2) are attached to "ground" and are solved with no modification to the large deflection equations. However, the other three joints (Joint 3, 6, and 7) are located between two moving links meaning that both ends are "free" and therefore have to be dealt with specially. The force angle ϕ and the desired joint angle θ_0, rather than just being functions of the link the joint is attached to, are functions of the difference between the two links they sit between. Doing this

"fixes" the base of the joint in space while only applying forces and moments to the free end, which is defined as the end of the joint that is furthest from the drive link. The same process is used for links D_4 and D_3 when modeling the soft link mechanism configuration as these links also sit between two other features.

2.3.2 Solving Foot Position Using the Psuedorigid-Body 1R Model

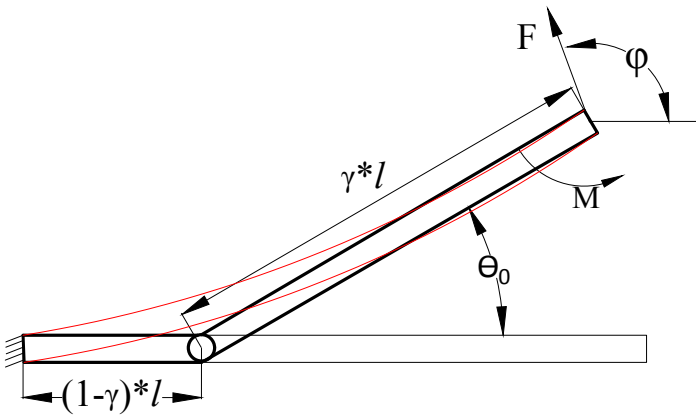

Figure 2.8: PRB 1R model showing γ in relation to soft component undeformed and deformed configuration. Red beam shows Large Deflection Beam Model setup overlaid

The classic 1R model simplifies the analysis for large deflections of compliant components by approximating the continuous member with two rigid links connected by a revolute joint with a torsional spring [29]. This method and the more advanced 3R model [27] assumes that the location of the revolute joint along the length of the soft component, which is determined by its length to width ratio and elastic modulus, is fixed for a given geometry and material. While this method works well for long and slender compliant beams, when the length to width ratio gets smaller, the accuracy decreases as the rotation center of the joint is more likely to change as the load ratio κ changes. With the load ratio κ determined in Sec. 2.3.1, a variable instantaneous center of rotation (IC) can be obtained using the PRB 1R model.

The location of the IC is determined by the characteristic radius factor γ as shown in Fig. 2.8. This figure shows the model setup for a single component with model parameters and loca-

tions detailed and an overlay of the Large Deflection Beam model so show comparison. The characteristic radius factor describes the location of the instantaneous center of rotation of the component. For example, a revolute joint has a $\gamma = 0.5$ which means that the rotation center is in the middle of the joint. Specifically for the 1R model, it has been shown that γ can be calculated from the load ratio κ, the optimal characteristic radius factors for pure end force (γ_F) and moment (γ_M), and a nonlinearity index c_γ [27]:

$$\gamma \approx \frac{\gamma_F + 2\gamma_M(c_\gamma \kappa)}{1 + 2c_\gamma \kappa} \tag{2.3}$$

where $\gamma_F = 0.842$ is the radius factor when pure force is applied at the tip (i.e., $M = 0$), $\gamma_M = 0.735$ is the radius factor when pure moment is applied (i.e., $F = 0$), and $c_\gamma = 4.694$ is an index obtained with linear regression using the relationship for κ and γ obtained from the Euler-Bernoulli beam model [27]. It is shown that the Eq. (2.3) can achieve an accuracy of 98%for estimating the γ [27].

The final step in the 1R model is to use the changing IC location calculated above to predict the new path of a point on the mechanism. The point of interest is the end of the final link where the leg contacts the ground. To determine the path of this point, a six-bar vector loop process (two sequential four bar loop equations) is used. Although the six-bar process is a standard method for solving mechanism motion, we have used the configuration-dependent length for links connected to soft joints (Joints 3 to 7) based on the IC location. To illustrate the general idea of obtaining the changing link length we used Link D_3 as an example in Fig. 2.9. This figure shows the setup for a portion of a mechanism with only soft joints. The same process is used for the soft link by simply adding the parameters of the soft link into the chain in the green section of length E. The length D_3 contains 3 parts in Eqn. 2.4. The first part of the equation takes into account the fixed length of the rigid link E. The second and third parts use the remaining portion of the joint that isn't fixed (γl). These are the values of γ that are based on the deflection angle θ_0 which is the current joint angle θ_4 minus the print angle ψ. The equation for how D_3 changes with respect to γ is as follows:

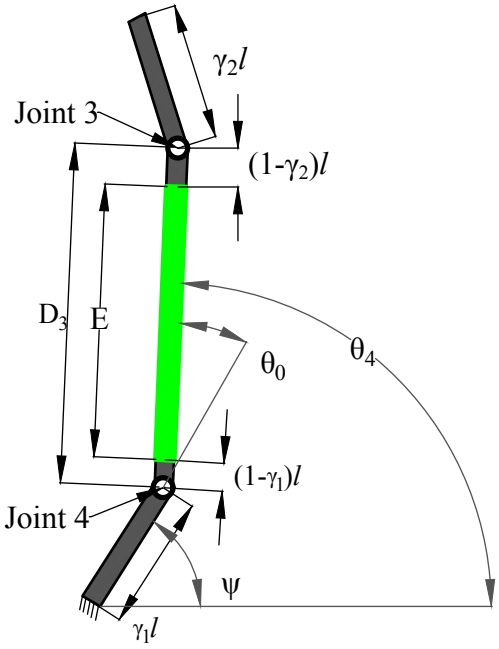

Figure 2.9: Link 3 (D_3) dimensioned showing variables in Eqn. 2.4, green represents the link and black the soft joints

$$D_3 = E + \gamma_1 l + \gamma_2 l \tag{2.4}$$

Link D_3 when modeled with the soft joint varies from 3.764 mm to 4.299 mm over a full rotation of the mechanism while it is fixed at 4.0625 mm when modeled as a revolute joint. A similar equation was used to incorporate the changing rotation center on all dimensions effected by γ. The layout of the first of the two four-bar vector loops is shown in Fig. 2.2 where θ_2 is the angle of the drive link and θ_4 is the angle being solved for. Equ. (2.5) represent a standard vector loop process that demonstrates how θ_4 is solved for [28].

$$\theta_4 = 2\arctan\frac{-B \pm \sqrt{B^2 - 4AC}}{2A} \tag{2.5}$$

where

$$A = K - \frac{D_8}{D_0} + \cos\theta_2$$
$$B = \frac{2D_7}{D_0} - 2\sin\theta_2$$
$$C = K + \frac{D_8}{D_0} - \cos\theta_2$$
$$K = \frac{D_1^2 - D_7^2 - D_8^2 - D_0^2 - D_3^2}{-2D_0D_3} - \frac{D_8}{D_3}\cos\theta_2 - \frac{D_7}{D_3}\sin\theta_2$$

This process gives the angle θ_4 based on θ_2. This is then used to find the path of Point 1 on the mechanism (see Fig. 2.2 for location). Then this process is repeated to find the next set of angles associated with D_4, D_5, and D_6 and finally the location of the Foot. The accuracy of the PRB 1R model, even at 98%, only means that we can estimate the deformation for an element that can be approximated with the Euler-Bernoulli beam model, where the axial deformation is not considered. It will be shown in Sec. 2.4 that even thought this model does not include this form of deformation, the error is acceptable as an estimation. But it is for this reason that the next numerical method was studied for increased accuracy and a wider variety of soft elements.

2.3.3 Solving Foot Position Using the Three Spring RPR Model

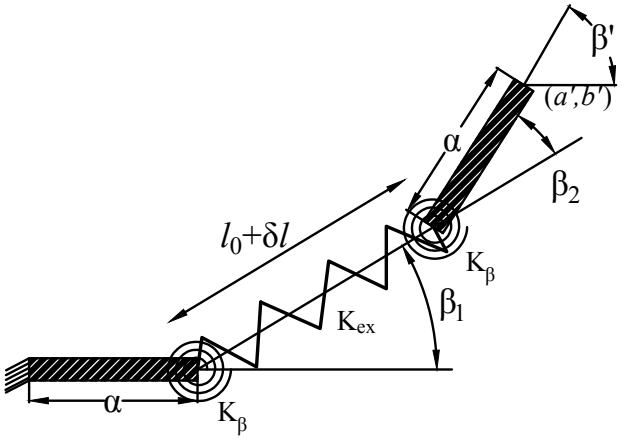

Figure 2.10: Three Spring RPR model showing parameters and variable layout

The Three Spring RPR model [21] approximates a continuous member as a serial chain of two links and three joints: a rigid link attached to the previous object, a revolute joint with a torsional spring at its center attached to the rigid link, a prismatic joint modeled as a linear spring from the first joint to the third joint, and a second revolute joint with a torsional spring attached to the free end of the member. Fig. 2.10 shows the schematic of the joint model with variables labeled. The length of the rigid section at each end of the member is α. K_β is the torsional spring constant of the spring at each revolute joint and K_{ex} is the spring constant of the linear spring. The linear spring of length $l_0 + \delta l$ is modeled such that it cannot bend, as if a prismatic joint was present, and it accounts for the axial deformation of the joint while the torsional springs account for the bending of the joint.

The RPR model satisfies five important criteria that make it ideal for the soft components used in the mechanism. First, it is able to predict a soft components end position and orientation under large deflections. Second, it takes into account axial deformation of a component. Third, it can handle a single inflection point in the components shape. Fourth, it is simple enough to be used in kinematics analysis of the mechanism. Fifth, all of the model parameters are load independent.

The parameters needed for this model are α, k_β, and k_{ex} which are dimensionless constants. The equations for K_β, K_{ex}, and l_0, which utilized these parameters, are as follows:

$$K_\beta = k_\beta \frac{EI}{L}, \quad K_{ex} = k_{ex} \frac{EA}{L}, \quad l_0 = L(1-2\alpha) \tag{2.6}$$

where E is the elastic modulus of the soft material, I is the moment of inertia, A is the cross-sectional area, and L is the length of the undeformed component. The non-dimensional parameters α, k_β, and k_{ex} are derived from the same method used by Venkiteswaran [21] who optimized the governing equations for the parameters and found appropriate values for each over a range of length-to-width ratios and best fit equations were obtained. The L-W ratio of the components in the designed mechanism fall outside the range studied in [21]. However, the best fit equations from [21] were still used to calculate the appropriate values for the constants

α, k_β, and k_{ex} for both the soft joints and soft links (Table 2.2). The results in both Sec. 2.4.1 and Sec. 2.4.2 prove that the best fit equations hold true to L-W ratios down to 0.94.

Table 2.2: RPR model parameters used for the two mechanism configurations

Component	L-W Ratio	α	k_β	k_{ex}
Soft Joint	0.94	0.007	2.011	1.075
Link D_3	2.56	0.126	2.018	1.059
Link D_4	3.45	0.178	2.016	0.975

When the external load $F = [F_x, F_y, M_z]^T$ from Sec. 2.3.1 is applied to the free end of a component, the reaction force/torque at that component in the RPR chain is calculated by:

$$\tau = J^T F \tag{2.7}$$

where $\tau = [K_\beta\beta_1, K_\beta\beta_2, K_{ex}\delta l]^T$ are the component forces and torques and J is the Jacobian of the RPR chain given by:

$$J = \begin{bmatrix} \alpha L[sin(\beta_2-\beta_1)]-(l_0+\delta l)cos\beta_1, & -sin\beta_1, & \alpha L[cos\beta_1 sin\beta_1 - cos\beta_2 sin\beta_1] \\ \alpha L[cos(\beta_1-\beta_2)]-(l_0+\delta l)sin\beta_1, & cos\beta_1, & \alpha L[cos(\beta_1-\beta_2)] \\ 1 & 0 & 1 \end{bmatrix} \tag{2.8}$$

Equ. 2.7 gives three equations with three unknowns: β_1, β_2, and δl. The three equations are solved simultaneously to get these unknowns. The location (a' and b') and orientation (β') of the component is solved using the forward kinematic equations of the component:

$$a' = \alpha L + (l_0 + \delta l)cos\beta_1 + \alpha L cos(\beta_1 + \beta_2) \tag{2.9}$$

$$b' = (l_0 + \delta l)sin\beta_1 + \alpha L sin(\beta_1 + \beta_2) \tag{2.10}$$

$$\beta' = \beta_1 + \beta_2 \tag{2.11}$$

Once the position and orientation of each soft component in the mechanism is solved, the values are used to solve for the trajectory of both Point 1 and the Foot of the mechanism. Fig. 2.11 illustrates how the RPR joint model is incorporated into the mechanism model containing soft joints only and how the joint variables β', a', and b' drive the mechanism motion. The same model (shown in the blowout circle) is implemented in place of the selected rigid links in the soft joint and soft links model. Since these variables account for the deformation of each component, a simple vector loop process using the position and orientation of all 5 soft components and the drive link is needed to solve for the desired paths.

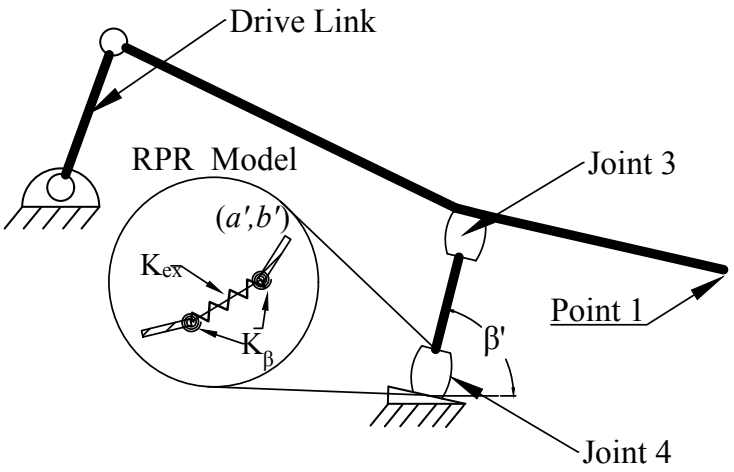

Figure 2.11: Three Spring RPR model shown in the fourbar section of the leg mechanism

2.4 Experimentation

To validate the models detailed above, physical experiments were conducted. These experiments began small with single legs tests on multiple joints designs, then full scale testing with the entire robot.

Once the single leg design was completed and leg trajectories were confirmed to be what was expected, a comparison test between a loaded and unloaded leg was conducted. This test was to confirm that our assumption that we can model the trajectory of the mechanisms with-

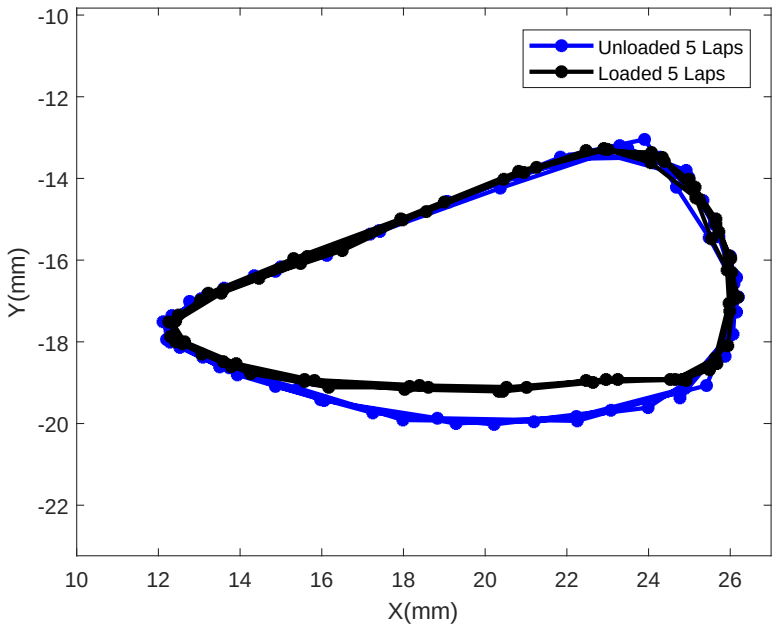

Figure 2.12: Five consecutive laps of experimental data for the loaded and unloaded case for leg with only soft joints.

out taking into account the weight of the robot and to show that the leg mechanism will repeatedly produce the same trajectory time after time. In the modeling, it is assumed that no external load is applied to the mechanism other than the torque from the drive joint. Such an assumption is reasonable as supported by experimental data for the foot trajectories with and without load for the leg with only soft joints. The experiment is conducted by putting the robot without the battery and electronics into a mount so that we can precisely control the robot's location. The robot is then set on top of a scale and pressed down on the scale until the exact weight for the walking robot is achieved. The robot legs are then driven and the foot trajectory collected. The scale is then removed, and the robot is driven to obtain the foot trajectory for this unloaded case.

Results of five laps for each case are shown in Fig. 2.12. From the comparison, we can see that the only difference for the trajectory is at the bottom part. It is almost flat in the loaded case since the leg contacts the ground, while it curves out a bit in the unloaded case since there is no ground to constrain the motion. Note that we expect the trajectories for leg with both

soft joints and links have a similar difference since the leg's dimensions remain the same. Since the bottom part in the trajectory will have a small impact on the walking capability, it is thus reasonable to develop a model without considering external loads. However, in the future, we will extend the models investigated in this paper to incorporate external loads. Additionally, the five sequential laps of each test show that the leg mechanism is repeatable and give validity to the bounds set on error in Sec. 2.4.1.

Next, experiments were conducted on the two robot leg configurations: soft joint only and soft joint and soft link. These tests are used to validate the numerical model trajectories and are backed up by defined error bounds and discussion of error sources and remedies.

2.4.1 Soft Joint Mechanism

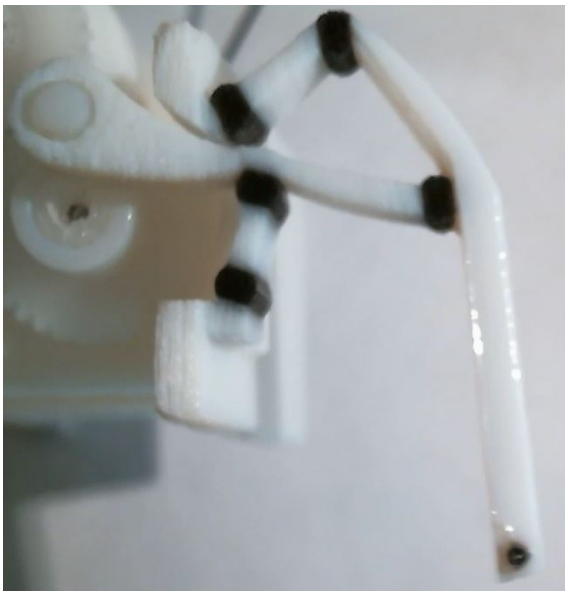

Figure 2.13: Image of soft joint mechanism configuration

The first version of the leg mechanism that is studied is the soft joint only mechanism. In this configuration, Joints 3 through 7 are printed in the 27A soft material while all the links are printed in the stiff plastic. Fig. 2.13 is an image of the single leg test stand with the soft joint mechanism. The black areas are the soft materials, the white is rigid plastic, and the black

point at the end of the mechanism the tracking point for video analysis. This configuration causes the least deviation from the path created by the revolute joint model. However, due to the material adhesion properties of the two different plastics, the boundary between the soft and rigid materials had a tendency to break apart after only a few cycles. With the limitations of the 3D printer, alterations of the boundary layer away from a flat rectangle is not currently feasible. Even with these initial design flaws, accurate experimental results are captured and compared to each numerical models predicted trajectory.

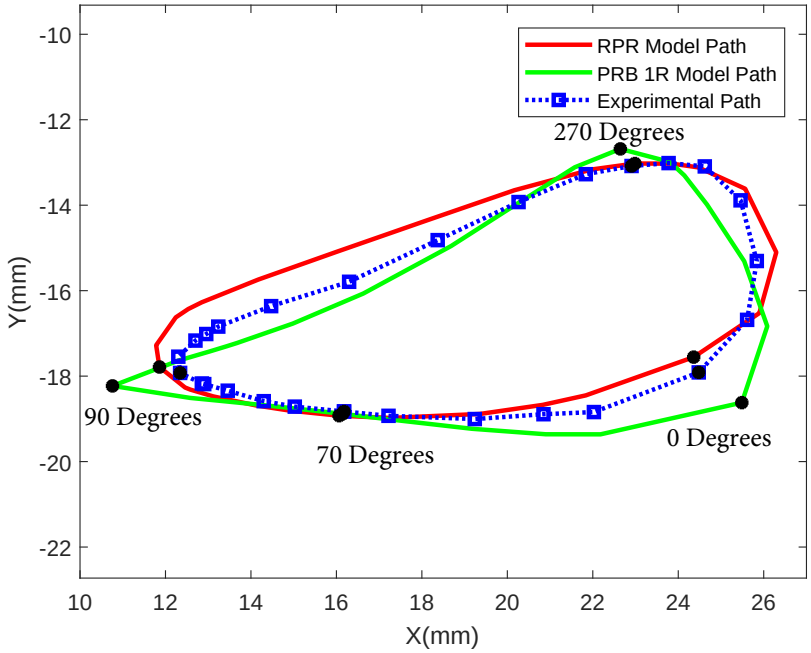

Figure 2.14: Plot of Foot path predicted by RPR model vs PRB 1R model vs Experimental results for the soft joint only configuration. Black markers show location in each trace at certain drive link angles. Print locations/starting location is 70 degrees.

To experimentally obtain the trajectory for the leg, we utilized video analysis by recording a video of the legs motion, and then manually obtaining the trajectory off-line by analyzing each frame from the video. To make video analysis more accurate, we printed a single leg on a test stand identical to one of the four legs in the robot. The experimental setup consisted of a Logitech C615 web-camera, a tripod with level bubble, test stand, a laptop, and an external power supply. The test stand was positioned on the table and set level to the table edge for a

horizontal reference. Then the camera was set level on the tripod about 50mm away from the test stand and a video was recorded by the laptop while the motor drove the leg. Once the video was collected, a video analysis software Tracker (physlets.org/tracker) was used to go frame by frame, track the foot, and plot its path.

The starting location of the trajectory, which is dictated by the print configuration of the mechanism and shown as the 70 degree mark in Fig. 2.14, must line up with model trajectory and while the particular shape of plots differ, the general shape and extents are gaged to be acceptable. Acceptable for the soft joint configuration of the mechanism for the Pt 1 plot was that the max straight line error between the experimental and model path was less than 2mm. Both the 1R and RPR models fall within the bounds and the trajectory of the foot of the mechanism is compared in Fig. 2.14. Once again the starting point for the trajectories was confirmed to be at its print location and the average and max errors for each model are calculated and presented in Table 2.3.

In order to confirm that a model can accurately predict the deformation of the soft joint in the mechanism and subsequently produce an accurate trajectory, an error bound on both average and max error is needed. The equation used to solve for the error at a single point in the trajectory is as follows:

$$error = \sqrt{(X_{exp} - X_{model})^2 + (Y_{exp} - Y_{model})^2} \tag{2.12}$$

For a foot position $[X_{exp}, Y_{exp}]$ in an image from the recorded video, we can also obtain the drive link angle in the image. This drive link angle is used for both the RPR and 1R model to obtain the $[X_{model}, Y_{model}]$ and used to match up the experimental foot location at specific angles with the model locations (see Fig. 2.14). The error is calculated at each experimental data point $[X_{exp}, Y_{exp}]$ along the path, and we list the average and maximum errors in Table 2.3. In this table is also listed the errors for a model that assumes all the joints in the mechanism use a traditional ideal revolute joints and rigid links.

Table 2.3: Soft Joint RPR model vs PRB 1R model vs Ideal model errors from experimental trajectory shown in Fig. 2.14

Foot Path Error	Average	Max
RPR Model	0.35 mm	0.54 mm
1R Model	0.43 mm	1.60 mm
Revolute Model	0.904 mm	5.5 mm

As Table 2.3 shows, both the RPR and 1R models fall within the stated error bounds and therefore can be validated as accurate representations of the soft joints in the mechanism. Note that the RPR model is able to reduce the max error by 67%, showing that the elongation and compression effects have a major impact on the deformation of the soft joints. With this increases accuracy, model speed is sacrificed. The time required to model the entire mechanism using the RPR model increases by 3 times over the 1R model. This is not very significant for the simple mechanism studied here but if applied to more complicated mechanism with more joints, the increased model time could have an impact.

2.4.2 Soft Link Mechanism

The second configuration of the leg mechanism studied has a combination of soft joints and soft and rigid links. For this model, the same joints as before are printed in the 27A soft material, while links D_3 and D_4 are printed in the more rigid 50A soft material. All other links are printed in rigid material and the overall geometry of the mechanism is unchanged from the soft joint only model. This configuration is studied because the boundary between the two soft materials is stronger than the boundary between the soft and rigid materials. This significantly increases the number of cycles the mechanism can undergo before failing. However, the introduction of soft links adds another level of complexity to the modeling process and changes the trajectory of the mechanism significantly away from the ideal trajectory originally designed. Fig. 2.16 shows

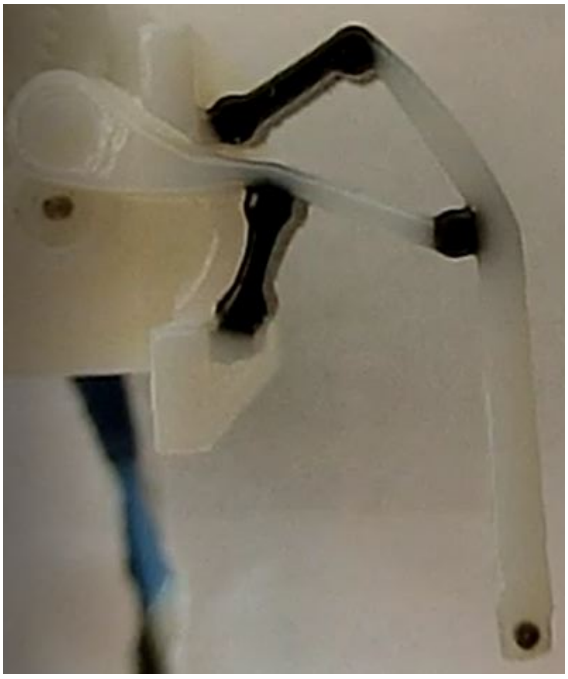

Figure 2.15: Image of soft link mechanism configuration

the trajectory of the foot of the mechanism with the RPR model shown in red, Experimental results in blue, and 1R model in green.

The same error bounds (max error less than 1.6mm and average error less than 0.5mm), error calculations, and data collection methods are used to evaluate the two models validity with the soft link mechanism configuration. The results of this study are very different than the soft joint configuration because the 1R model does not pass the accuracy requirements for the foot trajectory (See Table 2.4 for error values). Upon further investigation, link D_4 has an inflection point during a large section of its deformation which is not captured by the 1R model but is by the RPR model. Similar to the increase in model time seen with the soft joint only configuration, a 4 times increase in modeling time is observed between the 1R model and the RPR model. In this case, the added time is necessary to capture an accurate enough trajectory.

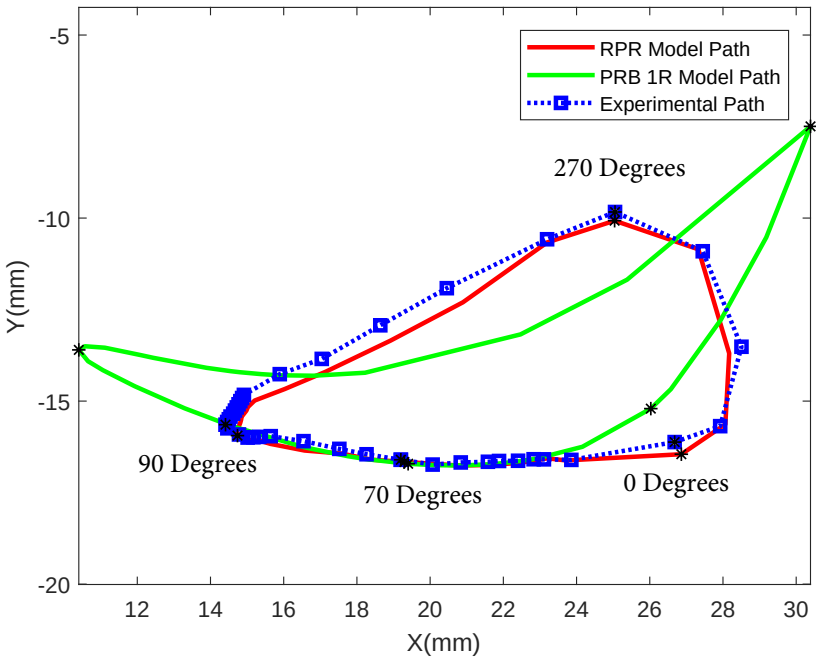

Figure 2.16: Plot of Foot path predicted with RPR model vs PRB 1R model vs experimental results for the soft joint and soft link configuration. Black markers show location in each trace at certain drive link angles. Print locations/starting location is 70 degrees.

Table 2.4: Soft Link RPR model vs PRB 1R model errors from experimental trajectory

Foot Path Error	Average	Max
RPR Model	0.26 mm	0.58 mm
1R Model	1.79 mm	6.20 mm
Revolute Model	1.66 mm	8.12 mm

Using the RPR model improves results in both leg configurations; however, some error still exists. There are three possible sources for the error. First, the RPR model is only an approximation to the deformation of soft elements to facilitate the mechanisms analysis procedure so that we can obtain a relatively accurate estimation in a timely fashion. In order to obtain more accurate predictions, more sophisticated models should be utilized (e.g., the Timoshenko beam

model [21]). Second, the force and moment required for the RPR model might not be accurate enough. They are obtained by assuming the mechanism has ideal revolute joints. An iterative procedure to use the derived deflection angle in the RPR model to solve the force and moment again might increase the precision, but at the cost of more computations. Third, the measurement procedure is not accurate enough with a webcam and a manual setup. Having a higher resolution camera with a faster frame rate would allow for more data points and more accurate video tracking.

2.4.3 Walking Capabilities

A final set of experiments are conducted to demonstrate the walking capabilities for the designed robot. Initially, the robot with legs having only soft joints is tested. However, due to the bonding issue between the soft and rigid materials, this robot does not complete walking capabilities testing. Instead, we test the robot with legs having both soft joints and links, which proves to be much more durable. With the legs running for almost one hundred cycles, no delamination in any joint or link is found. With the designs illustrated in Sec. 2.1, we assembled the robot with all the required parts for wireless remote control, including a lithium ion battery and a wireless controller, which had a onboard motor driver to control the robot to move either forward or backward. With the functional robot, we let it walk on a flat surface and record videos.

The results of these tests showed the robot could consistently move at 5.7cm/second or > 1 body length/second in both directions of motion. Still frames of the test are shown in Fig. 2.17. The weight of the motor, battery, and wireless controller together account for half the robot's total weight. As a result, careful positioning of these components is needed to ensure that the robot is properly balanced. Since the motor's position is fixed with the design, the battery and wireless controller can be placed at different locations on the robot to achieve the smoothest locomotion of the robot. The use of a smaller battery (e.g., the ultra low weight lithium ion batteries ($<$ 1gram) from PowerStream) and motor would reduce their percentage of the weight

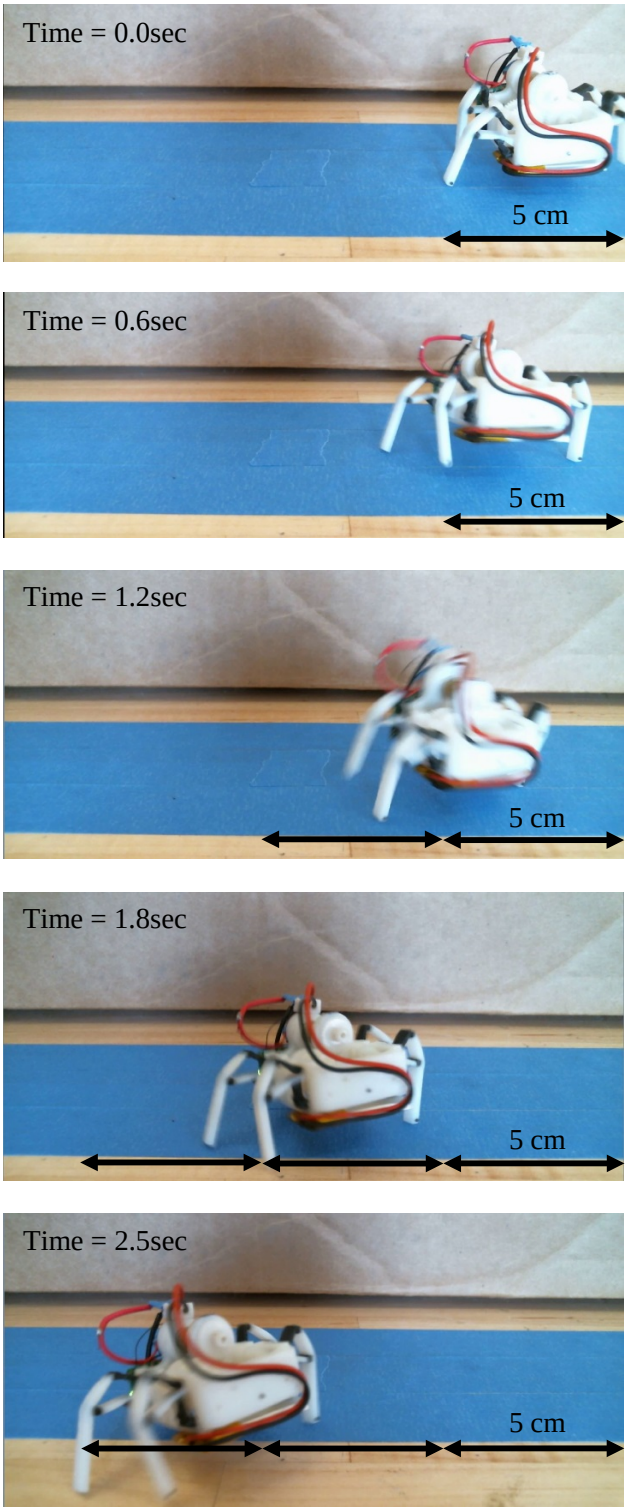

Figure 2.17: Sequential images of MM3D printed robot locomotion utilizing the soft joint and soft link leg configuration

and allow for more accurate balancing. While the locomotion speed of this robot is on the lower side when compared to other robots in this miniature category (See Sec. 1 for examples), those robots have been through multiple design cycles to achieve higher locomotion speeds and balance. The capabilities of the first prototype studied in this project prove that the use of 3D printed multi-material compliant mechanisms as walking mechanisms is a valid manufacturing and design method and should continued to be studied.

2.5 Summary

The goals for this portion of the project is to develop a walking robot prototype utilizing MM3D printing leveraging soft materials as compliant components in the place of traditional revolute joints and rigid links and develop numerical models to predict the motion of a mechanism that contains these 3D printed compliant parts. To this end, a miniature, four legged, walking robot was successfully manufactured, assembled and tested achieving a walking speed of greater than one body length per second, weighing less than 15 grams with a motor, battery, and wireless controller. Two numerical models were implemented and proved to be accurate enough to predict the alterations to mechanism behavior with multiple compliant members, one utilizing a variable rotation center (PRB 1R model) and another using multiple links and springs (RPR model) to approximate deformation.

Two configurations of the mechanism were modeled and tested, one with soft joints and rigid links and a second with both soft joints and soft links designed to increase the life of the mechanism. The RPR model successfully predicted mechanism behavior for both configurations while the 1R model was only able to capture the soft joint configuration. This is due to the significant axial deformation present in the soft links and the particular shape one of the links takes during deformation causing an inflection point in the curve.

This manufacturing and designing method not only validates the use of MM3D printing as a viable technique for printing miniature scale robots, it also proves that this process can be used on other previously designed mechanisms to replace the existing revolute joints and rigid links

with functional compliant components and understand the associated effects on trajectory and functionality.

Chapter 3

Mechanism Optimization

The custom designed Klann walking mechanism studied in the previous chapter fulfilled the original project goals of achieving a biomimetic walking motion using soft materials as compliant members in place of traditional revolute joints and rigid links and integrating multiple mechanisms into a functioning, miniature scale robot powered by a single motor. After multiple prototypes, a reliable platform has been developed for future research applications accompanied by a preferred numerical model developed to accurately predict the motion of a mechanism with compliant joints. Along with the characterization of the deformation properties of the soft joint, the numerical model has the adaptability to be integrated with an optimization routine to enhance the performance of the mechanism. There are three aspects of the design of a compliant mechanism that could benefit from optimization procedures. The first is the ability for the compliant mechanism to closely track the original trajectory of the mechanism before adding compliant features. Second is the reduction of force needed to move the compliant features through a cycle. Third is to reduce the maximum deflection of the compliant feature. This research focuses on the first two properties and specifically on the optimization of compliant mechanisms that are directly designed to match existing mechanisms. The goal of this work is to optimize the link lengths of the compliant mechanism so that the output of the mechanism closely matches the output of the original revolute joint mechanism designed in Sec. 2.1. This work will show the ability to simulate complaint mechanisms that can follow the trajectory of a previously designed mechanism without drastically altering its configuration and being able to implement compliant features into existing mechanisms and keep similar mechanism functionality.

This chapter progresses as follows. First, the setup for the optimization routine is detailed with assumptions, penalty functions and the setup for two different optimization outcomes: overall best trajectory and best result at specific locations. Second, the results of the two opti-

mization routines run on the soft joint only configuration of the leg mechanism are presented and discussed. Third, the results of the two optimizations routines applied to the soft joint and soft link mechanism are presented and discussed. Finally, all the results are summarized and a recommended optimization technique for these types of compliant mechanism is given.

3.1 Optimization Process

The chosen optimization routine for this work is the built in fminsearch function in MATLAB. This optimization routine uses the Nelder-Mead simplex algorithm which searches values of the desired function around the initial guess, chooses the smallest value and repeats the process till the function value does not change, resulting in the local minimum of the function. The function minimized comes from the work done by [3] who re-designed well known mechanism with flexible joints made with long, slender rods of 3D printed plastic. This paper uses the following equation to track how closely the predicted mechanism trajectory matches the desired or original trajectory by measuring the x and y distance from each optimized foot location to the desired foot location at the same drive link angle:

$$ftrack = 0.5\sum[(X_{error})^2 + (Y_{error})^2] \tag{3.1}$$

Two different variations of this equation were tested, each trying to optimize the paths in different ways. The first and most common penalties added to optimization functions are bounds to keep the optimized values within a certain range ensuring that a solution is not found outside the physical constraints of the mechanism. This results in the following form of Eqn. 3.1:

$$ftrack = 0.5\sum[(X_{error})^2 + (Y_{error})^2] + penalty1 + penalty2 + penalty3 \tag{3.2}$$

where

$$penalty1 = rp * max(0, D_0 - 4) + rp * max(0, 2.75 - D_0)$$

$$penalty2 = rp * max(0, D_3 - 4.1) + rp * max(0, 2.75 - D_3)$$

$$penalty3 = rp * max(0, D_4 - 6) + rp * max(0, 2.75 - D_4)$$

and $rp = 100$ is the penalty multiplier, D_0, D_3, and D_4 refer to links in Fig.2.2, and the bounds within the $max()$ refer to the longest and shortest lengths each link can be without further altering the mechanism design (ex. altering the location of the ground links and joints, location of motor and gears). The second adjustment is selecting the locations on the trajectory that are most important to the mechanism function and adding penalties to the errors associated specifically with those points rather than the entire path. The points selected for this routine are shown in Fig. 3.1 showing their location on both the desired trajectory and the non-optimized trajectory that was achieved using the design in the previous chapter. Adding these penalties turns Eqn. 3.1 into the following:

$$ftrack = ftrack1 + ftrack2 + ftrack3 \tag{3.3}$$

where

$$ftrack1 = |X(1)_{error}| + |Y(1)_{error}|$$

$$ftrack2 = |X(2)_{error}| + |Y(2)_{error}|$$

$$ftrack3 = |X(3)_{error}| + |Y(3)_{error}|$$

This equations adds together the distance from the desired to the modeled foot location at each of the three desired locations with equal weighting. It was determined to keep equal weighting on the three locations so as to not vary too many variables in a single test without the ability to determine which had the desired impact.

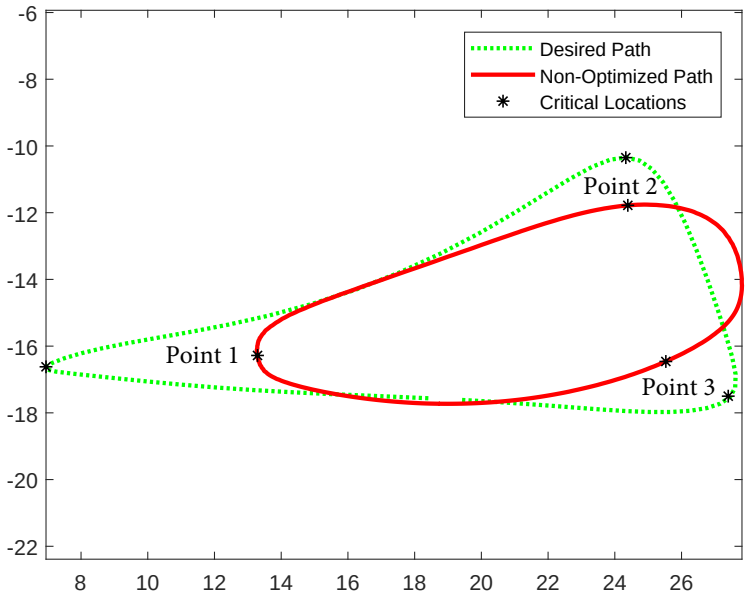

Figure 3.1: Location of important path locations on desired mechanism trajectory vs non-optimized trajectory

Each iteration of the optimization routine goes as follows. First, the chosen values for the link lengths are used to solve for the vector of angles for each joint in the mechanism. Second, those angles are used in the Large Deflection Beam Equation (Sec. 2.3.1) to determine the forces associated with each joint during a complete cycle of the drive link. Third, the forces are used in the Three Spring RPR joint model (Sec. 2.3.3) with the chosen link lengths and the output of the mechanism is calculated. The RPR method was chosen as the numerical model over the PRB 1R model as it was able to more accurately predict the motion of all compliant features even thought it is a more numerically intensive processes. Fourth, the simulated trajectory is compared against the desired trajectory using either Eqn. 3.2 or Eqn. 3.3. Finally, the value of $ftrack$ is returned to the optimization solver and new link lengths are selected.

The two mechanism configuration studied in previous sections are each optimized using both methods and compared to determine which method produces the best result for this research. Best is defined as the method that can produce a trajectory that best replicated the functionality of the desired trajectory. This includes shape, orientation and extents of the path.

3.2 Optimizing Soft Joint Mechanism

The soft joint only configuration is the most simple simulation as there are only five soft joints whose forces and deflections need to be calculated. This configuration shows how a previously designed mechanism can be very easily redesigned to replace the existing revolute joints with soft joints without altering the overall geometry. By optimizing from this configuration, the simple modifications to an existing mechanism can be determined to minimize the overall effects of the soft joints on the desired trajectory. This optimization determines the best values for three main links in the chain: D_0, D_3 and D_4, without altering the geometry of the soft joints. Refer to Sec. 2.1.1 for link locations in mechanism. Figure 3.2 shows the comparison between the the optimized trajectory, the desired mechanism trajectory, and the non-optimized trajectory used as the starting point for the optimization using Eqn. 3.2 as the minimizing function and Fig. 3.3 compares the trajectories using Eqn. 3.3. From these images, it can be seen that the utilization of the soft joints results in the inability to precisely match the desired trajectory of a similar revolute joint mechanism. However, by optimizing just a few link lengths, a close approximation of the trajectory is possible. In the case of the walking robot studied in the previous chapters, the alteration to the foot trajectory has a minimal impact on the ability of the mechanism to perform the task it was designed to do.

Table 3.1 shows the starting values and the optimized values for each equation used. Additional tests were performed using random initial values, far from the local minimum values found in the first tests, to test the accuracy of the final values and each case returned numbers that were within 5% of the values shown in the table. The most drastic change is the length of D_3 for both cases showing that this dimension has the greatest impact on generating the trajectory needed as well as being the length furthest from the ideal value.

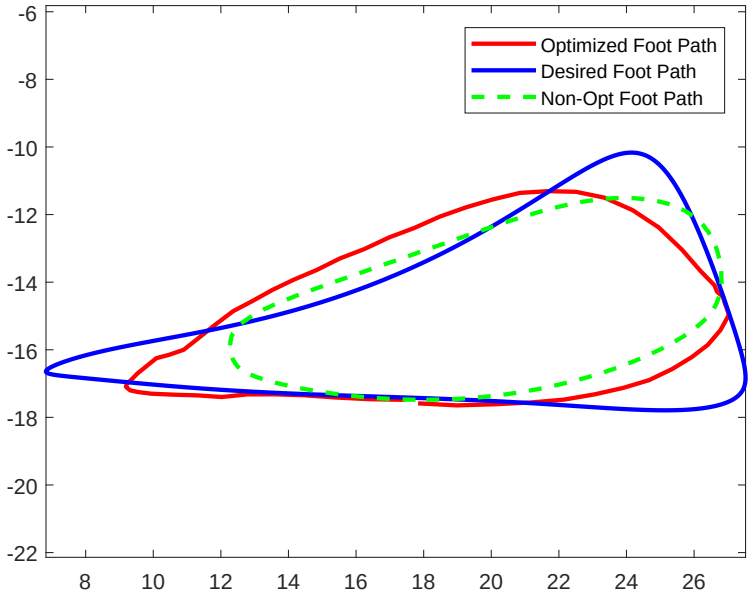

Figure 3.2: Desired vs Optimized vs Non-Optimized trajectory of soft joint configuration utilizing Eq.3.2

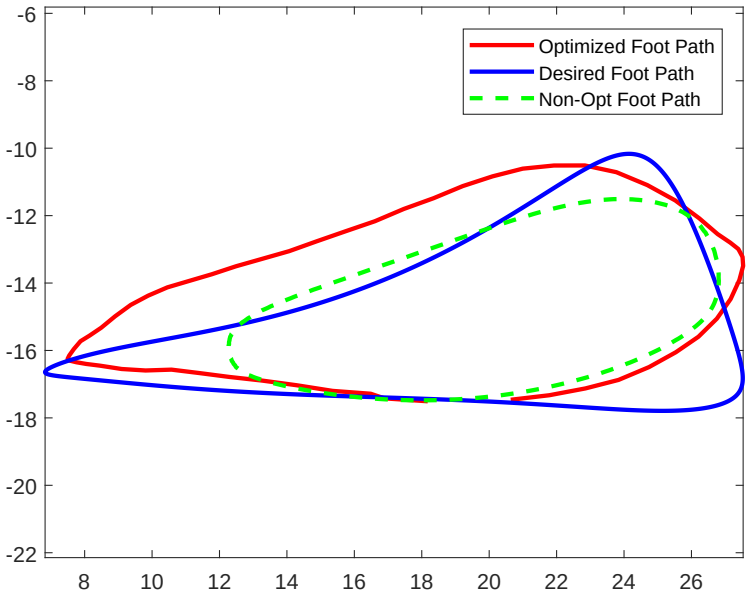

Figure 3.3: Desired vs Optimized vs Non-Optimized trajectory of soft joint configuration utilizing Eq. 3.3

Table 3.1: Table of optimized values for soft joint mechanism

Opt. Variables	D_0	D_3	D_4
Inital Values	3.44	4.06	5.31
Eqn. 3.2	3.31	3.35	4.83
Eqn. 3.3	3.68	3.70	5.34

3.3 Optimizing Soft Link - Soft Joint Mechanism

The second configuration of the mechanism is more complicated than the first. This configuration consists of the same soft joints as the previous optimization but replaces two rigid links with soft material while keeping the same geometry. This model is much more computationally extensive, as the addition of each soft link requires the same amount of calculation time as three soft joints due to the three links and three springs present in model Three Spring RPR model.

This model optimizes the same three link lengths as the previous optimization: D_0, D_3 and D_4 using both the overall best path method and closest to the desired three points method. Table 3.2 details the starting and ending values for the optimized links. With the same starting link lengths as the Soft Joint only configuration, strikingly similar link lengths were determined. Even though the link lengths are very close to the same, the soft links in this configuration cause very different optimization results. The trajectories in Fig. 3.4 and Fig. 3.5 are quite different from their soft joint only counterparts. Fig. 3.4 show a less rounded path that seems to better follow the desired path in various places however it only achieves a marginally better result than the soft joint configuration. The trajectory utilizing the 3 defined locations for optimization improves significantly on the best overall when it comes to following the shape of the desires path.

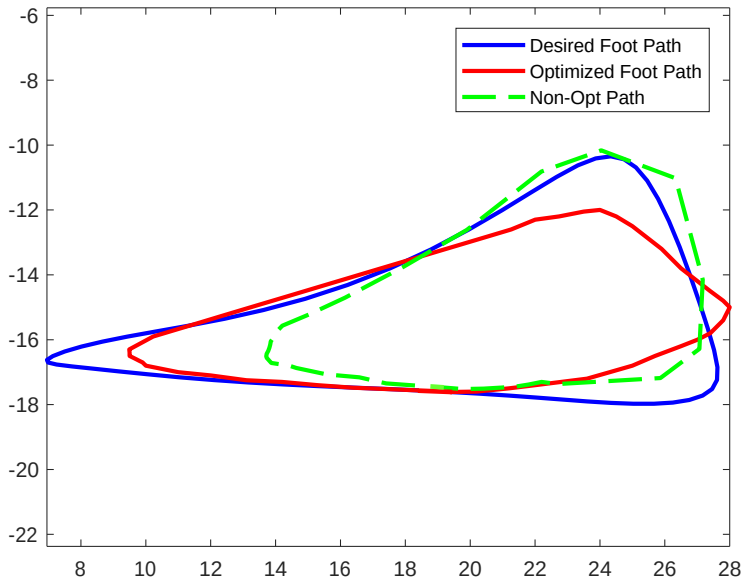

Figure 3.4: Desired vs Optimized vs Non-Optimized trajectory of soft joint-soft link configuration utilizing Eq. 3.2

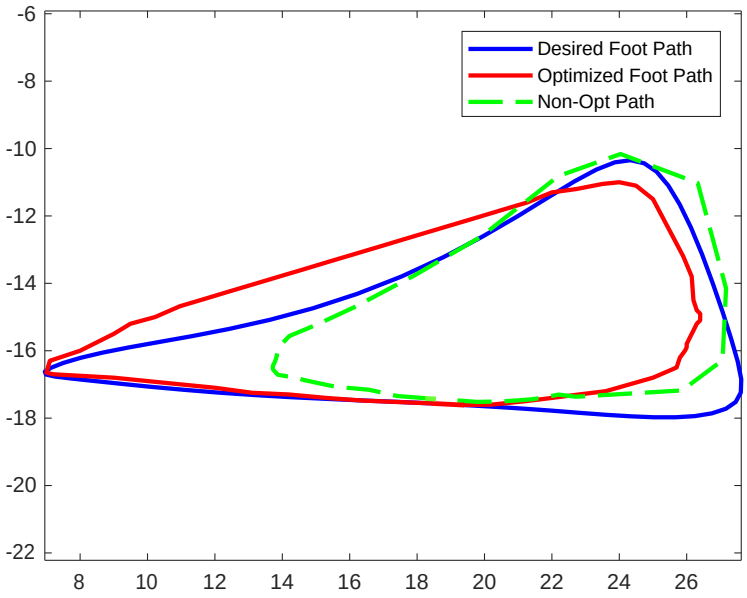

Figure 3.5: Desired vs Optimized vs Non-Optimized trajectory of soft joint-soft link configuration utilizing Eq. 3.3

Table 3.2: Table of optimized values for Soft Joint-Soft Link mechanism configuration

Opt. Variables	D_0	D_3	D_4
Inital Values	3.44	4.06	5.31
Eqn. 3.2	3.40	3.30	4.92
Eqn. 3.3	3.67	3.79	5.67

3.4 Optimization Summary

Utilizing simple optimization routines into the design and modeling of compliant mechanisms gives great insight into the impact that each link in a compliant mechanism has on the overall output of the mechanism. The first configuration of the mechanism studied, which contains only soft joints, has the ability to create trajectories similar to a desired trajectory but the alterations to the mechanism are limited unless an optimization of the joint geometry is also incorporated. The second configuration of the mechanism, containing both soft joint and soft links, is able to generate significantly better optimized trajectories over the soft joint only configuration. Both optimization strategies produce more accurate paths. The variability in the soft links creates more variation in the mechanism trajectory with a small change to link lengths and drives the final mechanism closer to the desired trajectory.

When comparing optimization strategies, the results are mixed. The time to optimize each configuration was independent of the method used. No noticeable differences in time were see between the best full path and the three critical locations. The soft joint configuration path using best path method is able to better replicate the shape of the desired trajectory, however the 3 critical points method pushes the path far outside the desired. The soft joint - soft link configuration does optimize to a closer shape using the 3 critical points. The decision comes down to the intended use of the compliant mechanism. If the mechanism needs to perform specific functions at specific locations, that clearly make the critical points method the preferred method as this bring those points on the desired and optimized as close together as possible. In the case of the mechanism designed for this research, the mechanism is intended for walk-

ing and therefore the trajectory above the ground has minimal impact to the effectiveness of the mechanism. The "best" result would give a maximum flat length of path at the bottom of the cycle, giving maximum contact with the ground. Based on this requirement, for both the soft joint and soft joint - soft link configurations, the three critical locations method (Eqn. 3.3) proves to be the best method.

Chapter 4

Adaptive 3D Printed Compliant Mechanism with Variable Joint Locations

The continuing advances in printer technology and materials has given way to multi-material 3D printing and has opened a new realm of manufacturing and design capabilities not previously available to everyone. Along with these major advances in the field specifically in the technology, more simplistic changes have occurred in standard 3D printer material used in spool fed, single material printers that are revolutionizing the functionality of entry level printers. Recently, a few manufacturers of 3D printing plastics have introduced conductive 3D printer materials that print the same base materials as before but are integrated with a conductive material that allows for the flow of electricity within the part. These filaments are either ABS or PLA based with come kind of conductive material infused into it. When printed, the material will conduct electricity with fairly well defined resistive properties both between layers and within the same layer. These materials are advertised as having uses in electronics, giving the ability to print parts that will conduct electricity to various components but with conductivity comes resistance. For this PLA material, if the temperature is above the so-called "glass transition temperature", then the material will become soft. Directly apply electricity to conductive PLA will increase its temperature and create the soft joint or link [30].

This chapter involves the study of the use of conductive carbon infused PLA by Proto-Pasta[3] as the material used to 3D print compliant mechanisms. The idea behind using this material for links in a mechanism is that if electrical resistance can be used to heat and soften the material, any section of a rigid link can be turned into a soft joint. With this ability, the trajectory of a mechanism could be altered without human intervention and without changing the configuration, the length, or the number of links present. The same mechanism could walk with a gait3

[3] https://www.proto-pasta.com/pages/conductive-pla

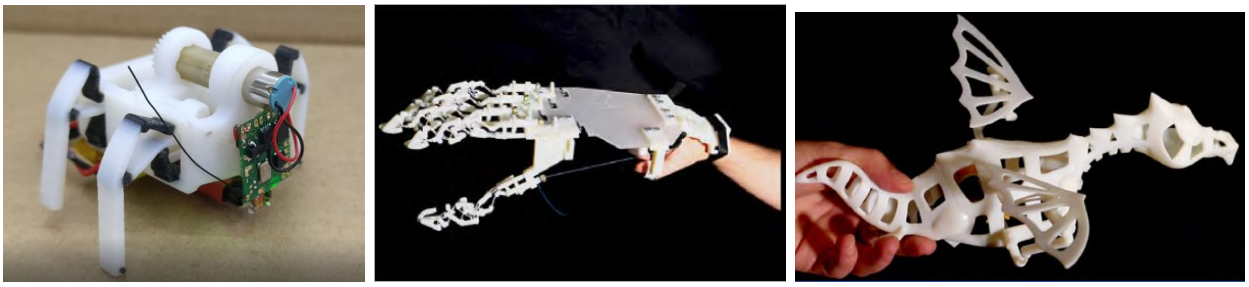

(a) **(b)** **(c)**

Figure 4.1: Various tasks that could be combined into a single mechanism: walking (a), gripping [3] (b), 3D flapping wing [3] (c)

optimized for flat terrain (Fig. 4.1a), a gait that is optimized for rough terrain, be used to grasp and hold an object (Fig. 4.1b) or even be used for a 3 dimensional flapping wing mechanism (Fig. 4.1c) in conjunction with either of the previous applications.

There are two goals for this preliminary study. First, we want to determine the voltage required to soften the material without burning and that the material will remain in tact when deformed in its softened state. The second goal is to develop a platform that allows testing of various joint configurations as well as testing of the durability of the material and the practicality of utilizing the material for various applications. The first section of this chapter will detail the design of the various testing components as well as the robotic testing platform. The second section will review the preliminary results of study and general observations on functionality and design. Last is a summary of the results, discussion of future research applications, and lessons learned.

4.1 Design

The design objectives for this study are to design a mechanism that contains at least two different locations for soft joints that exist within the rigid links that will hold together when turned to soft joints, create the least impact on the original mechanism trajectory, have a mechanism that can produce both a walking trajectory and an arc trajectory, and create a four legged robot

with the mechanism that can walk and grip an object as well as test future configurations of the links and joints.

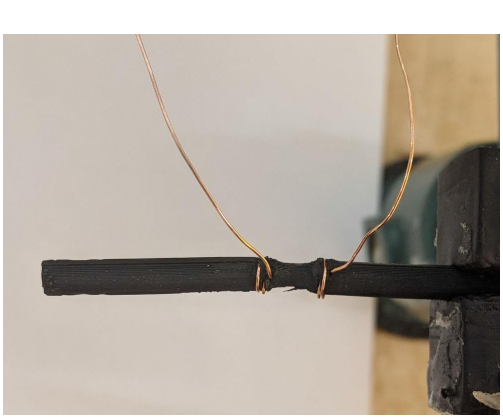

(a) 0 degrees

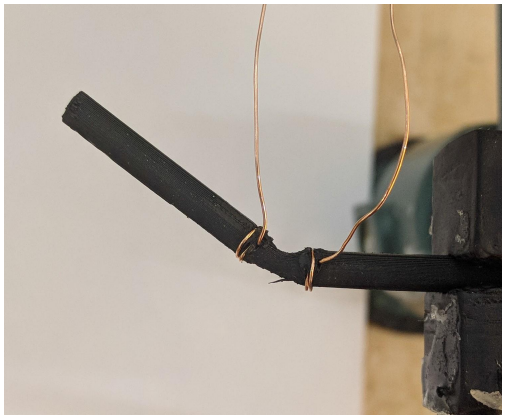

(b) 45 degrees

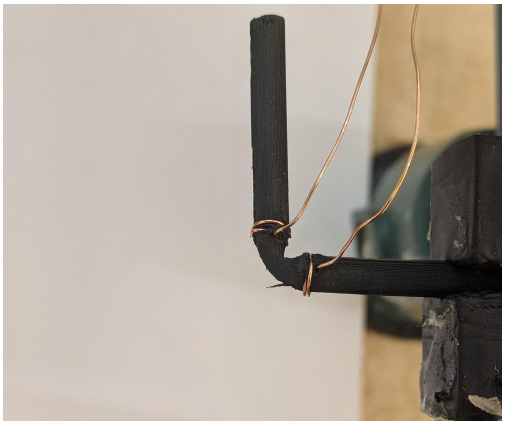

(c) 90 degrees

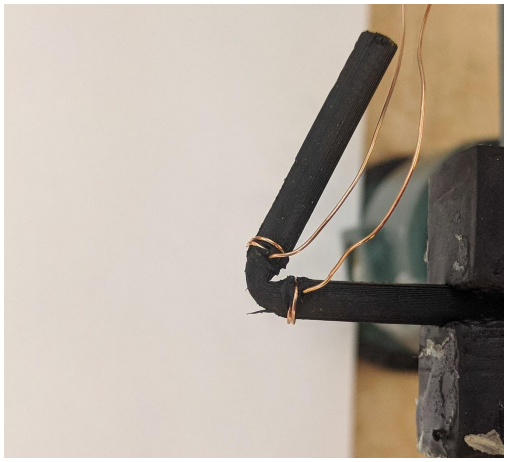

(d) 120 degrees

Figure 4.2: Conductive PLA compliant joint test link

The test link shown in Fig. 4.2 is a $25mm$ long, $4mm$ diameter cylinder printed in conductive PLA. The joint is located in the center of the link and is $3mm$ at the smallest and gradually builds out to the $4mm$ cylinder diameter. This design was chosen because it allows for easy testing of three dimensional motion with the joint, the axis of rotation is very near the center of the joint, and the part can be printed in under 10 mins on a Lulzbot Mini desktop printer allowing for quick iterations. To apply voltage to the joint, 32awg solid copper wire is wrapped around each

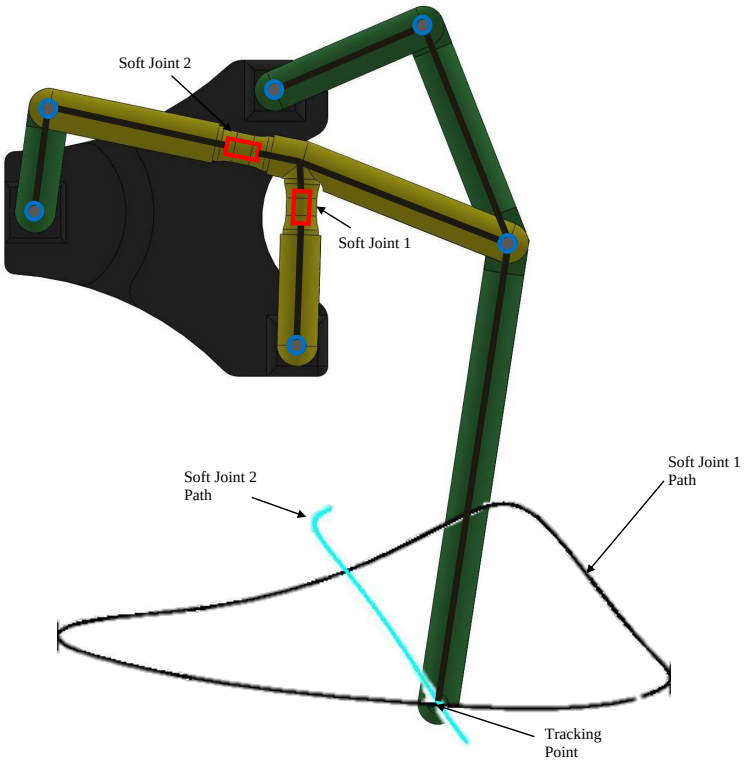

Figure 4.3: Variable trajectory mechanism with soft joint call-outs and designed trajectories for each joint configuration

end of the joint and a hot soldering iron is used to heat the copper and melt the wire into the surface of the link to allow for maximum conduction. By trial and error, $11V$ was determined to be the optimal voltage to soften the joint without melting or burning the material. When the joint is rigid and electricity is applied, the link pulls a maximum of $60mA$ and settles at $9mA$ when the joint is soft. Each joint is able to bend up to approximately 120° from it print orientation before it will not return to the original shape.

To simplify the design of the mechanism, the custom walking linkage (Fig. 2.2) studied in the previous chapters was used as the starting point. The overall size was scaled up by three since size is not a critical design parameter at this stage and through a design study of the impact of each link dimension of the trajectory of the mechanism, the location of the two test joints, the length of all links and location of all base joints were determined. Only two joints are realized as soft joints, one to create the walking trajectory and one to create the arc or gripping trajectory,

the remainder are designed as revolute joints to isolate the joint testing to one soft joint at at time. Fig. 4.3 shows the linkage configuration showing joint location and the two trajectories that the linkage should produce.

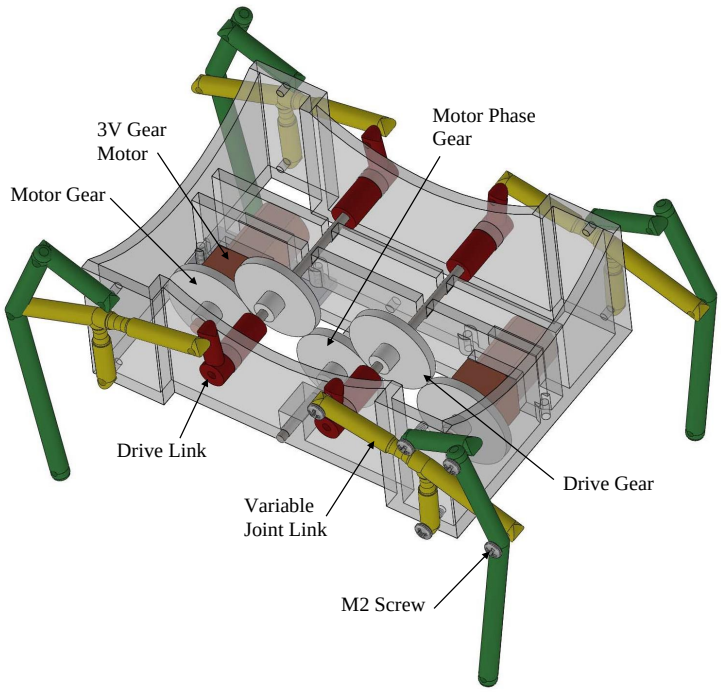

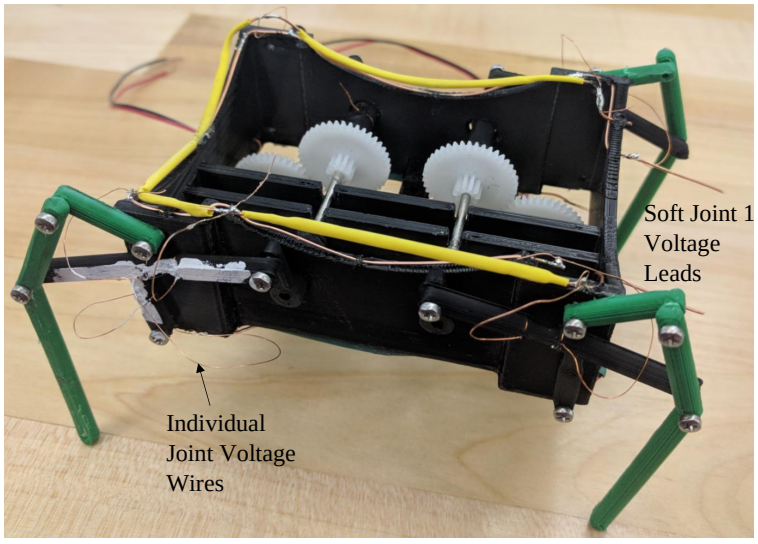

Figure 4.4: Four legged robotic test platform showing component locations

The robot test platform shown in Fig. 4.4 has the same leg layout as the multi-material robot studied earlier, with a rectangular body and a leg at each corner oriented like crab. Each leg has two soft joint locations, each with two wires. Around the top and bottom of the perimeter of the robot, a bare and insulated wire is run to solder each wire to. At each end of the robot, two of the main wires terminate so that applying a voltage to the wires on the left makes the first joint soft on all link and applying it to the wires of the right make the second joint soft. Each revolute joint in each linkage is realized using M2 machine screws. The legs are driven by two 3V 30RPM geared DC motors, one to drive the front and one to drive the back legs. Two motors are needed because to walk, all four legs need to be driven in the same direction and to grip, the front and back legs have to be driven i n opposite directions. Stainless steel $2mm$ shafts are used to connect the drive links to the drive gears which are meshed with the motor gear. To ensure that during walking the motors do not get out of phase, an idler gear is placed between the two drive gears and is removed to perform the gripping tests. The same walking gait detailed in Sec. 2.1.2 is used for the walking design of the robot.

4.2 Variable Function Testing

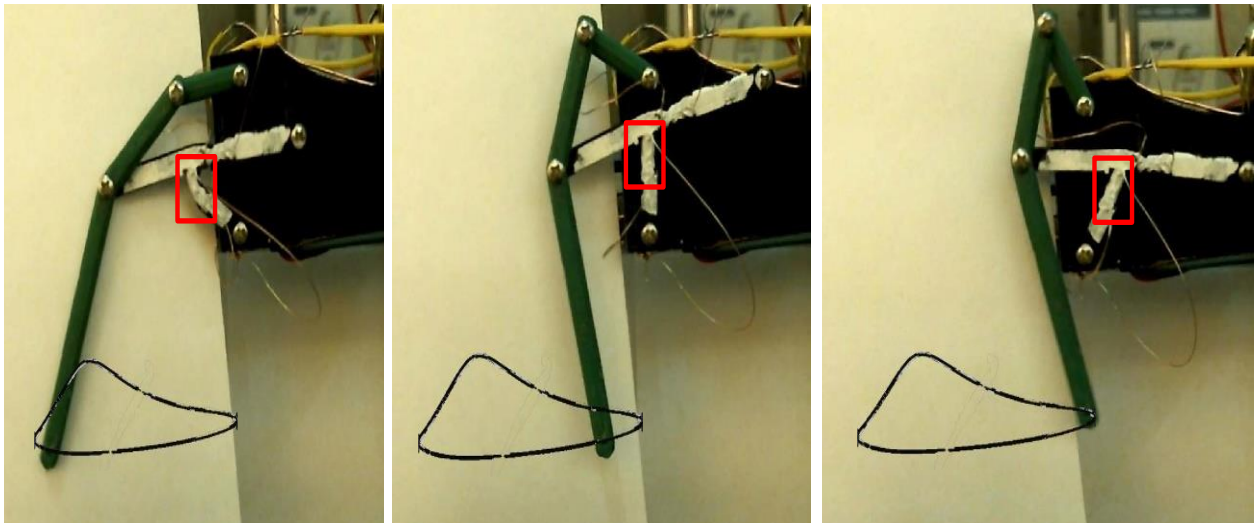

Figure 4.5: Single leg test stand at various angles during testing of walking configuration, highlighting three drive link angles. The soft joint location is highlighted with the red box.

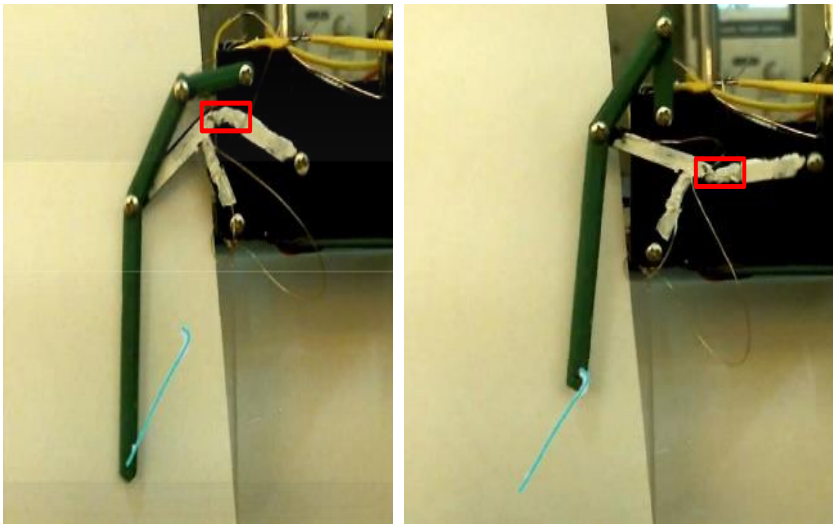

Figure 4.6: Single leg test stand at various angles during testing of gripping configuration, highlighting two drive angles. The soft joint location is highlighted with the red box.

Three separate tests are conducted to determine first the feasibility, then the design of the adaptive compliant mechanism. The first test involves the single leg test stand in Fig. 4.5 and Fig. 4.6 where $11V$ is applied to each of the soft joint locations one at a time and the drive link is rotated by hand to control the speed and force during testing. Fig. 4.5 shows the mechanism with the drive link at 90° , 180° , and 270° . Each joint takes about 10 sec to become soft once electricity is applied and 10 sec to cool down before becoming fully rigid again. This testing proves that the soft joint deforms as expected creating the intended leg trajectories and will not break or pull apart. The mechanism underwent at least 50 rotation cycles and 10 heating and cooling cycles without failure.

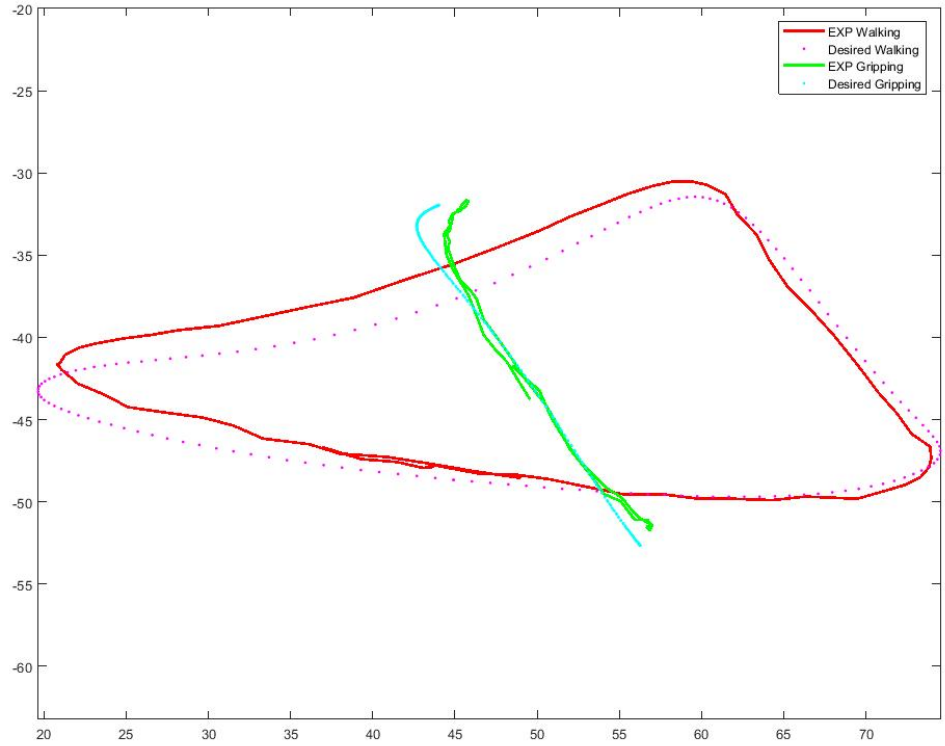

Figure 4.7: Plot of desired vs experimental trajectories for variable joint mechanism

A similar process as was used in Sec. 2.4 where a single leg was positioned infront of a stationary camera and a video was taken and analyzed to determine the true mechanism trajectory. Fig. 4.7 shows the results of the trajectory analysis of the two paths created by the mechanism. This figure shows that the desired trajectory was maintained with each joint configuration. Since the other 6 joints in the mechanism are revolute joints, it is expected that the trajectory would be similar to the designed. However, the experimental results give promise to the ability for an entire mechanism realized with conductive PLA to produce trajectories to the accuracy of the multi-material mechanism (Sec. 2.4.2).

The second and third experiments test the ability for the robotic platform with four variable joint mechanisms to accomplish sustained walking capabilities and gripping abilities without alteration and minimal human intervention. For the second experiment, the robot was placed on a soft blanket to provide a higher coefficient of friction between the legs and the ground. 11

volts was applied to the first soft joint location on all four legs and the two motors powered the robot to walk in a stable fashion at a speed of 2 cm/sec which was mainly governed by the speed of the motors. Faster speed could be achieved by incorporating a faster motor or a higher gear ratio. Fig. 4.8 shows still frames taken during the locomotion testing. This testing shows that the soft joints are able to transfer the force of the drive motor to the move the robot without failing while still replicating the walking trajectory of each leg.

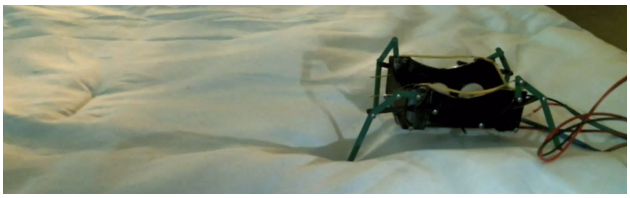

(a)

(b)

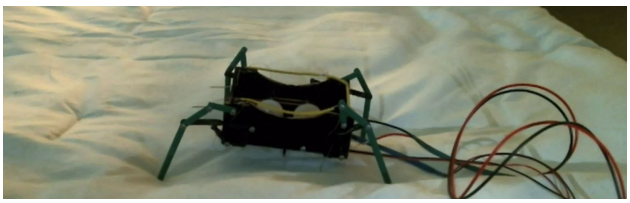

(c)

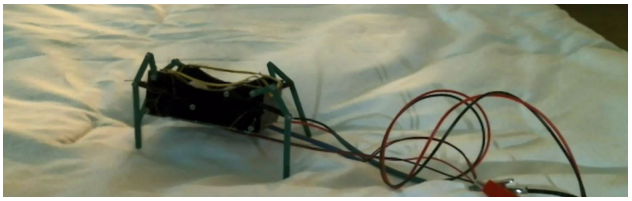

(d)

Figure 4.8: Sequential walking images at (a) 0 *sec*, (b) 3 *sec*, (c) 6 *sec*, (d) 9 *sec* of adaptive joint mechanism

For the third experiment, the robot was suspended from a test stand with a rectangular piece of foam located between the four legs and the idler gear removed from between the motors.

Voltage was applied to the second soft joint and all four legs were driven simultaneously bringing all legs into contact with the foam. The motors were driven till they stalled which gripped the foam firmly enough that the foam could not be removed without the risk of damaging the legs in the process (Fig. 4.9). The test was repeated three times, beginning to ensure durability of the joints.

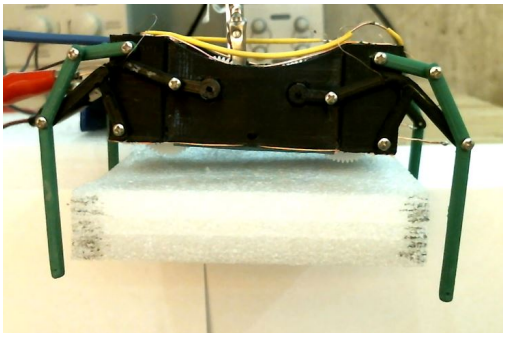

(a)

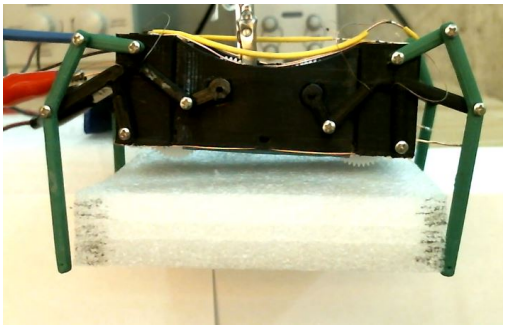

(b)

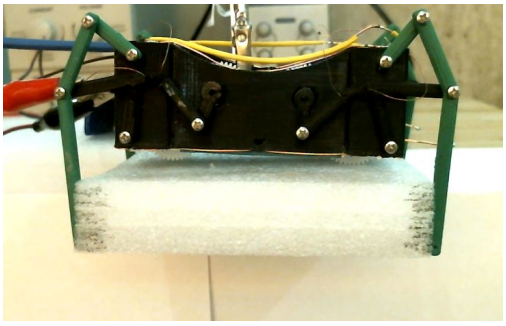

(c)

Figure 4.9: Sequential gripping images of adaptive joint mechanism

4.3 Summary

Overall, both goals were successfully tested and confirmed as feasible. The designed joints are able to soften in a quick and repeatable fashion, deform without failure while creating usable trajectories, and multiple trajectories could be achieved with the same mechanism without alteration to design or setup. During all three sets of tests, no joints failed or had to be repaired. The conductive PLA proved to be even more durable than the multi-material joints studied earlier, however more force was required to rotate the mechanism in the walking configuration than a similarly scaled multi-material mechanism. The method of transmitting voltage through exposed copper wire was not ideal as the wires have the potential to short out if they touch and after repeated motion, the wire did crease and break. Future design should look at how to integrate the wires inside or along the links.

This is the first prototype of this robot platform utilizing conductive 3D printer material to create an adaptive compliant mechanism. Now that the concepts has been proven to be feasible, continued research on the project should follow to further investigate the possible uses as well as develop more robust joint designs and entire mechanisms utilizing the soft joints. A wide range of possible applications for this research exist including further design of variable gait walking robots, flying robot with adaptive wing mechanisms and walking mechanisms that can directly incorporate the existing design being able to walk and grip and variable diameter wheeled robots.

Chapter 5

Conclusion and Future Work

In this thesis, the design, fabrication, modeling, testing, and optimization of a centimeter-scale walking robot is presented. Different from existing miniature walking robots, the presented robot can be directly fabricated using the multi-material 3D printing (MM3P) technology with soft material for the joint and certain links and rigid material for other parts. A modified Klann mechanism is adopted for each of the four legs, and with MM3P, all the leg mechanisms were be fabricated with the body of the robot. As the soft joints in the studied mechanism are different from traditional compliant joints, a numerical method is developed to analyze the motion trajectories for mechanisms with soft joints focusing on capturing both the rotational and axial deformation of the joints. Experimental results on a single leg's motion verified the effectiveness of two proposed numerical models and parameters to help chose which model to use going forward, while walking experiments demonstrated the robot's locomotion capabilities. The optimization of the linkage design through numerical simulation shows the versatility of the Three Spring RPR numerical model and the ability to create compliant mechanisms specifically with soft components that can closely replicate existing rigid link mechanisms. Additionally, the design and testing of a compliant mechanism shows how, utilizing a conductive PLA material, the same mechanism used for walking robots can be further utilized to create various other trajectories without altering the design or impairing the original functionality while having the possibility of increasing the durability of the robot.

The results presented in this thesis could lead to multiple continuing research avenues, a few of which are detail next. While the RPR joint model is accurate enough for these preliminary studies, a more refined model should be studied. Specifically, a more analytically based model that does not rely so heavily on numerical approximation. This would help to decrease computation time and increase the overall accuracy, making the way for further study of direct implementation of soft components into previously design rigid mechanisms.

With the validation of concept for adaptive soft joint mechanisms utilizing conductive PLA, further study of a similar application into 3D mechanisms such as flapping wing mechanisms could be studied. Along with this, designing a smaller platform that test new mechanism trajectories and be mounted to a UAV to being to combine the functionality of a flying robot with the added benefit of being able to walk, grip, and perch without adding the unnecessary weight of additional motors or multiple mechanisms.

Bibliography

[1] A.Rexaei Mojdehi, M. Alitavoli, and A. Darvizeh. Kinematic simulation of spider's walking by image processing. *International Conference on Information and Computer Science*, pages 3–6, 2009.

[2] Frederico L. Moro, Alexander Spröwitz, Alexandre Tuleu, Massimo Vespignani, Nikos G. Tsagarakis, Auke J. Ijspeert, and Darwin G. Caldwell. Horse-like walking, trotting, and galloping derived from kinetic motion primatives (kmps) and their application to walk/trot transitions in a compliant quadruped robot. *Biological Cybernetics*, pages 309–320, 2013.

[3] Vittorio Megaro, Jonas Zehnder, Moritz Bächer, Stelian Coros, Markus Gross, and Bernhard Thomaszewski. A computation design tool for compliant mechanisms. Technical report, Disney Research, July 2017.

[4] Aaron M Hoover, Erik Steltz, and Ronald S Fearing. Roach: An autonomous 2.4 g crawling hexapod robot. In *2008 IEEE/RSJ International Conference on Intelligent Robots and Systems*, pages 26–33. IEEE, 2008.

[5] Nicholas J Kohut, Aaron M Hoover, Kevin Y Ma, Stanley S Baek, and Ronald S Fearing. Medic: A legged millirobot utilizing novel obstacle traversal. In *Robotics and Automation (ICRA), 2011 IEEE International Conference on*, pages 802–808. IEEE, 2011.

[6] Paul Birkmeyer, Kevin Peterson, and Ronald S Fearing. Dash: A dynamic 16g hexapedal robot. In *2009 IEEE/RSJ International Conference on Intelligent Robots and Systems*, pages 2683–2689. IEEE, 2009.

[7] Andrew T Baisch, Onur Ozcan, Benjamin Goldberg, Daniel Ithier, and Robert J Wood. High speed locomotion for a quadrupedal microrobot. *The International Journal of Robotics Research*, 33(8):1063–1082, 20014.

[8] Ryan St Pierre and Sarah Bergbreiter. Gait exploration of sub-2 g robots using magnetic actuation. *IEEE Robotics and Automation Letters*, 2(1):34–40, 2017.

[9] RJ Wood, S Avadhanula, R Sahai, E Steltz, and RS Fearing. Microrobot design using fiber reinforced composites. *Journal of Mechanical Design*, 130(5):052304, 2008.

[10] Mark R Cutkosky and Sangbae Kim. Design and fabrication of multi-material structures for bioinspired robots. *Philosophical Transactions of the Royal Society of London A: Mathematical, Physical and Engineering Sciences*, 367(1894):1799–1813, 2009.

[11] Aaron M Dollar and Robert D Howe. A robust compliant grasper via shape deposition manufacturing. *IEEE/ASME transactions on mechatronics*, 11(2):154–161, 2006.

[12] Sangbae Kim, Jonathan E Clark, and Mark R Cutkosky. isprawl: Design and tuning for high-speed autonomous open-loop running. *The International Journal of Robotics Research*, 25(9):903–912, 2006.

[13] Wojciech Bejgerowski, John W Gerdes, Satyandra K Gupta, and Hugh A Bruck. Design and fabrication of miniature compliant hinges for multi-material compliant mechanisms. *International Journal of Advanced Manufacturing Technology*, 57(5):437, 2011.

[14] Wojciech Bejgerowski, John W Gerdes, Satyandra K Gupta, Hugh A Bruck, and Stephen Wilkerson. Design and fabrication of a multi-material compliant flapping wing drive mechanism for miniature air vehicles. In *ASME International Design Engineering Technical Conferences and Computers and Information in Engineering Conference, Montreal, QC, Canada, Aug*, pages 15–18, 2010.

[15] Dana E Vogtmann, Satyandra K Gupta, and Sarah Bergbreiter. Multi-material compliant mechanisms for mobile millirobots. In *Robotics and Automation (ICRA), 2011 IEEE International Conference on*, pages 3169–3174. IEEE, 2011.

[16] Dana E Vogtmann, Satyandra K Gupta, and Sarah Bergbreiter. Characterization and modeling of elastomeric joints in miniature compliant mechanisms. *Journal of Mechanisms and Robotics*, 5(4):041017, 2013.

[17] Andrew T Gaynor, Nicholas A Meisel, Christopher B Williams, and James K Guest. Multiple-material topology optimization of compliant mechanisms created via polyjet three-dimensional printing. *Journal of Manufacturing Science and Engineering*, 136(6):061015, 2014.

[18] Arnaud Bruyas, François Geiskopf, and Pierre Renaud. Design and modeling of a large amplitude compliant revolute joint: The helical shape compliant joint. *Journal of Mechanical Design*, 137(8):085003, 2015.

[19] Arnaud Bruyas, François Geiskopf, and Pierre Renaud. Toward unibody robotic structures with integrated functions using multimaterial additive manufacturing: Case study of an mri-compatible interventional device. In *IEEE/RSJ International Conference on Intelligent Robots and Systems (IROS)*, pages 1744–1750. IEEE, 2015.

[20] Nicholas W Bartlett, Michael T Tolley, Johannes TB Overvelde, James C Weaver, Bobak Mosadegh, Katia Bertoldi, George M Whitesides, and Robert J Wood. A 3d-printed, functionally graded soft robot powered by combustion. *Science*, 349(6244):161–165, 2015.

[21] Venkatasubramanian Kalpathy Venkiteswaran and Hai-Jun Su. A three-spring pseudorigid-body model for soft joints with significant elongation effects. *Journal of Mechanisms and Robotics*, 8(6):061001, 2016.

[22] Kevin Y Ma, Pakpong Chirarattananon, Sawyer B Fuller, and Robert J Wood. Controlled flight of a biologically inspired, insect-scale robot. *Science*, 340(6132):603–607, 2013.

[23] Venkatasubramanian Kalpathy Venkiteswaran and Hai-Jun Su. Extension effects in compliant joints and pseudo-rigid-body models. *Journal of Mechanical Design*, 138(9):092302, 2016.

[24] Joseph C Klann. Walking device, November 12 2002. US Patent 6,478,314.

[25] Kazuo Morita and Hidenori Ishihara. Proposal of 4-leg locomotion by phase change. In *Climbing and Walking Robots*, pages 517–524. Springer, 2006.

[26] Seonggi Kim, Cho-long Jung, Youngdo Jung, Hyungpil Moon, and Hyuneui Lim. Biomimetic skin-type shear sensor. pages 1331–1332, 2016.

[27] Hai-Jun Su. A psuedorigid-body 3r model for determining large deflection of cantilever beams subject to tip loads. *ASME Journal of Mechanisms and Robotics*, 1:021008–1, 2009.

[28] Robert L. Norton. *Design of Machinery*. McGraw-Hill, 5th edition, 2012.

[29] Larry L Howell. *Compliant Mechanisms*. John Wiley & Sons, 2001.

[30] Mohammed Al-Rubaiai, Thassyo Pinto, David Torres, Nelson Sepulveda, and Xiaobo Tan. Characterization of a 3d-printed conductive pla material with electrically controlled stiffness. In *ASME 2017 Conference on Smart Materials, Adaptive Structures and Intelligent Systems*, pages V001T01A003–V001T01A003. American Society of Mechanical Engineers, 2017.